

Award Number: W81XWH-12-2-0055

TITLE: Sub-lethal Ocular Trauma (SLOT): Establishing a Standardized Blast Threshold to Facilitate Diagnostic, Early Treatment, and Recovery Studies for Blast Injuries to the Eye and Optic Nerve

PRINCIPAL INVESTIGATOR: Walt Gray, Ph.D., Matthew Reilly, Ph.D.

CONTRACTING ORGANIZATION: University of Texas at San Antonio,
San Antonio, TX 78249

REPORT DATE: September 2013

TYPE OF REPORT: Annual Report

PREPARED FOR: U.S. Army Medical Research and Materiel Command
Fort Detrick, Maryland 21702-5012

DISTRIBUTION STATEMENT: Approved for Public Release;
Distribution Unlimited

The views, opinions and/or findings contained in this report are those of the author(s) and should not be construed as an official Department of the Army position, policy or decision unless so designated by other documentation.

REPORT DOCUMENTATION PAGE

Form Approved
OMB No. 0704-0188

Public reporting burden for this collection of information is estimated to average 1 hour per response, including the time for reviewing instructions, searching existing data sources, gathering and maintaining the data needed, and completing and reviewing this collection of information. Send comments regarding this burden estimate or any other aspect of this collection of information, including suggestions for reducing this burden to Department of Defense, Washington Headquarters Services, Directorate for Information Operations and Reports (0704-0188), 1215 Jefferson Davis Highway, Suite 1204, Arlington, VA 22202-4302. Respondents should be aware that notwithstanding any other provision of law, no person shall be subject to any penalty for failing to comply with a collection of information if it does not display a currently valid OMB control number. **PLEASE DO NOT RETURN YOUR FORM TO THE ABOVE ADDRESS.**

1. REPORT DATE September 2013			2. REPORT TYPE Annual			3. DATES COVERED 15 August 2012-15 August 2013			
4. TITLE AND SUBTITLE Sub-lethal Ocular Trauma (SLOT): Establishing a Standardized Blast Threshold to Facilitate Diagnostic, Early Treatment, and Recovery Studies for Blast Injuries to the Eye and Optic Nerve						5a. CONTRACT NUMBER			
						5b. GRANT NUMBER W81XWH-12-2-0055			
						5c. PROGRAM ELEMENT NUMBER			
6. AUTHOR(S) Walt Gray, Matthew Reilly, Brian J. Lund, William E. Sponsel, Randolph D. Glickman E-Mail: walter.gray@utsa.edu						5d. PROJECT NUMBER			
						5e. TASK NUMBER			
						5f. WORK UNIT NUMBER			
7. PERFORMING ORGANIZATION NAME(S) AND ADDRESS(ES) University of Texas at San Antonio One UTSA Circle San Antonio, TX 78249						8. PERFORMING ORGANIZATION REPORT NUMBER			
9. SPONSORING / MONITORING AGENCY NAME(S) AND ADDRESS(ES) U.S. Army Medical Research and Materiel Command Fort Detrick, Maryland 21702-5012						10. SPONSOR/MONITOR'S ACRONYM(S)			
						11. SPONSOR/MONITOR'S REPORT NUMBER(S)			
12. DISTRIBUTION / AVAILABILITY STATEMENT Approved for Public Release; Distribution Unlimited									
13. SUPPLEMENTARY NOTES									
14. ABSTRACT The report summarizes the results of tasks undertaken during Year 1 of the project "Sub-lethal Ocular Trauma (SLOT): Establishing a Standardized Blast Threshold to Facilitate Diagnostic, Early Treatment, and Recovery Studies for Blast Injuries to the Eye and Optic Nerve." The 3 year effort aims to fill a gap in our understanding of physical mechanisms and progression of primary blast-induced ocular injury. A fully-integrated experimental and computational study was undertaken. Primary blast experiments were conducted using a large diameter shock tube and <i>ex vivo</i> porcine eye specimens. The experiments were supported by numerical modeling using physics-based codes CTH and LS-DYNA. Post-blast evaluation of eye specimens using UBM and B-scan, as well as gross dissection and detailed histopathology, allowed for preliminary development of trauma risk curves for a number of sub-globe-rupture trauma categories. The data generated in this study has increased our understanding of primary blast-induced ocular trauma. The shock tube produced a broad array of closed-globe injuries such as angle recession, cyclodialysis, peripheral chorioretinal detachments, radial peripapillary retinal detachments, and internal scleral delaminations. Development of a rigorous experimental methodology and use of pre-blast ultrasound screening gave confidence that the observed injuries were due to the effects of primary blast.									
15. SUBJECT TERMS Ocular Trauma, Primary Blast, Shock Tube Experiments, Trauma Prediction, <i>ex vivo</i> Porcine Model, Numerical Modeling									
16. SECURITY CLASSIFICATION OF:						17. LIMITATION OF ABSTRACT	18. NUMBER OF PAGES	19a. NAME OF RESPONSIBLE PERSON USAMRMC	
a. REPORT U		b. ABSTRACT U		c. THIS PAGE U				19b. TELEPHONE NUMBER (<i>include area code</i>)	
						UU	51		

ANNUAL REPORT
**Sub-lethal Ocular Trauma (SLOT): Establishing a Standardized Blast
Threshold to Facilitate Diagnostic, Early Treatment, and Recovery
Studies for Blast Injuries to the Eye and Optic Nerve**

Prepared For:

U.S. Army Medical Research and Materiel Command
Fort Detrick, Maryland 21702-5012

Prepared by:

Walt Gray; Ph.D.
Matthew Reilly; Ph.D.
Department of Biomedical Engineering
University of Texas at San Antonio
One UTSA Circle
San Antonio, TX 78249-0663

Brian J. Lund; Ph.D.
Ocular Trauma Division
U.S. Army of Institute of Surgical Research
3698 Chambers Pass, Building 3610
Joint Base San Antonio
Ft. Sam Houston, TX 78234-6315

William E. Sponsel; Ph.D., M.D.
WESMD Professional Associates
311 Camden, Suite 306
San Antonio, TX 78215

Randolph D. Glickman; Ph.D.
Department of Ophthalmology
University of Texas Health Science Center- San Antonio
7703 Floyd Curl
San Antonio, TX 78229-3900

Submitted: 14 September 2013

ABSTRACT

This report summarizes the results for all tasks undertaken during Year 1 of the project “Sub-lethal Ocular Trauma (SLOT): Establishing a Standardized Blast Threshold to Facilitate Diagnostic, early Treatment, and Recovery Studies for Blast Injuries to the Eye and Optic Nerve.” The project is funded by the U.S. Army Medical Research and Materiel Command as Vision Research Program (VRP) Grant W81XWH-12-2-0055. The 3 year effort aims to fill a gap in our understanding of the physical mechanisms and progression of primary blast-induced ocular trauma. Although ocular injuries resulting from penetration of blast-driven fragments and debris (secondary blast) are well documented and understood, injuries resulting from only the air shock or blast wave (primary blast) have to date received little attention.

Our approach is a fully-integrated experimental and computational study; with blast experiments conducted using the U.S. Army Institute of Surgical Research (ISR) large diameter shock tube, and experiments fully supported with computational analysis using physics-based codes CTH and LS-DYNA. The simulations carefully mimic the experiments with the goal of fully reproducing the trauma observed in the experiments. Experiments increase in complexity from *ex vivo* porcine eyes in Year 1 of the study to *in vivo* rabbit eyes in Year 2. Use of the *in vivo* rabbit model will allow for biochemical marker monitoring and characterization. The project will culminate in Year 3 with development of trauma predictive models. The data generated during the experiments will be used to formulate empirical models useful in predicting the probability of observing a number of sub-globe-rupture injuries under various blast pressure-impulse or energy environments.

Tasks completed to date include (1) development of detailed procedures for preparation and blast testing of eye specimens and the conduct of 68 shock tube experiments on porcine eyes, (2) completion of preliminary pathology on 96 porcine eye specimens, (3) preliminary development of trauma risk curves for a number of sub-globe-rupture trauma categories, (4) preliminary numerical simulations using software packages CTH and LS-DYNA, and (5) recovery and mounting of optic nerve specimens in preparation for imaging using the Matrix Assisted Laser Desorption Ionization (MALDI) technique.

The project is being undertaken as a collaborative research effort between personnel from the University of Texas at San Antonio, the U.S. Army Institute of Surgical Research (Ocular Trauma Division), the University of Texas Health Science Center-San Antonio, and the Sponsel Professional Association of San Antonio. The data and predictive models generated to date have significantly increased our understanding of blast-induced ocular injury. The shock tube produced a broad array of closed-globe injuries, many of which would seriously compromise visual function. The experimental techniques and injury characterization methodologies offer an objective assessment as to which injuries were due to primary blast exposure.

TABLE OF CONTENTS

	<u>Page</u>
1. INTRODUCTION.....	1
2. SUMMARY OF RESEARCH.....	6
2.1 Blast Experiments.....	6
2.2 Shock Tube.....	8
2.3 Porcine Eye Specimen Preparation.....	10
2.4 Pathology.....	13
2.5 Biomarker Study.....	18
2.5.1 Optic nerve studies in ex vivo porcine eyes.....	19
2.5.2 Retina and optic nerve investigations in cadaver rats.....	22
2.6 Trauma Data Analysis and Modeling.....	22
2.7 Numerical Models and Simulation.....	26
2.7.1 LS-DYNA.....	28
2.7.2 CTH.....	32
3. KEY RESEARCH ACCOMPLISHMENTS.....	36
4. REPORTABLE OUTCOMES.....	37
5. CONCLUSIONS.....	38
6. REFERENCES.....	40
APPENDIX I Porcine Eye Blast Experiments Matrix.....	44
APPENDIX I Summary of Porcine Blast Experiments	46

1. INTRODUCTION

It has been estimated that in the Iraq and Afghanistan conflicts eye injuries account for more than 13% of all combat injuries; the highest rate since World War I and the fourth most common injury among deployed personnel (Weichel et al., 2010). Blast-related injuries are commonly classified as primary (shock and air pressure effects), secondary (penetration from blast-driven fragments and debris), tertiary (blunt impact after blast acceleration), and quaternary (primarily heat and explosive gas toxicity). Penetration, contusion, and laceration by fragments and blast-driven debris (secondary) accounts for over 82% of all combat ocular injuries (Mader et al., 2004; Thach et al., 2008). Penetration-type injuries are readily observable so the trauma mechanisms are well documented and understood. However, a significant number of injuries may also result from explosive overpressure alone (primary blast) resulting in internal ocular injuries that may not be easily recognized. Although blast injury and effects to other major body organs have been reasonably well characterized (Bowen et al, 1968; Stewart, 2006; Stuhmiller, 2008a), primary blast-related trauma to the eye has not been extensively studied. The high incidence of ocular injuries relative to its small areal exposure suggests that the eye may be especially vulnerable to blast injury. High energy blast weapons such as improvised explosive devices (IEDs) will become an ever increasing threat to U.S. military personnel in future conflicts, thus knowledge of primary blast effects on the eye takes on increased importance. Currently, protective eyewear available through the Military Combat Eye Protection Program (MCEP) provides ballistic or fragment protection, but not protection from the potentially harmful effects of blast overpressure. Thus, a large gap exists in our understanding of physical mechanisms and progression of blast-induced ocular trauma. This gap hampers our ability to extend the design of effective protective devices, and may contribute to ineffective treatment and rehabilitation due to inadequate awareness of potentially vision-threatening injury.

A non-penetrating blunt impact study conducted at Southwest Research Institute (SwRI) demonstrated that progression of ocular trauma is well correlated with impact energy (Gray, et al, 2008a; Gray et al., 2008b; Sponsel et al., 2011). The research showed that significant internal damage could occur without obvious external evidence. The study used porcine specimens as surrogates for the human eye and highly deformable paintballs to ensure that the impact energy was imparted to the eye without penetration. Until globe rupture occurred (~10 J) internal damage was not typically evident from external examination. However, detailed post-impact pathology revealed that, at significantly lower energies (2-7 J), internal trauma could be severe including cyclodialysis, iridodialysis, angle recession, lens displacement, as well as retinal and choroid detachment. Using paintball mass (m_p) and velocity, an approximate correlation between impact energy ($E = \frac{1}{2}m_pV^2$) and trauma severity can be shown (Figure 1). The previous blunt impact study (Gray et al., 2008a; Sponsel et al., 2011) treated injury in a qualitative way, as there were insufficient test repetitions (at each injury level) to allow for estimation of ocular injury and incapacitation probabilities (at a given energy of impact).

Paintball Impact Ocular Trauma Thresholds (Porcine)

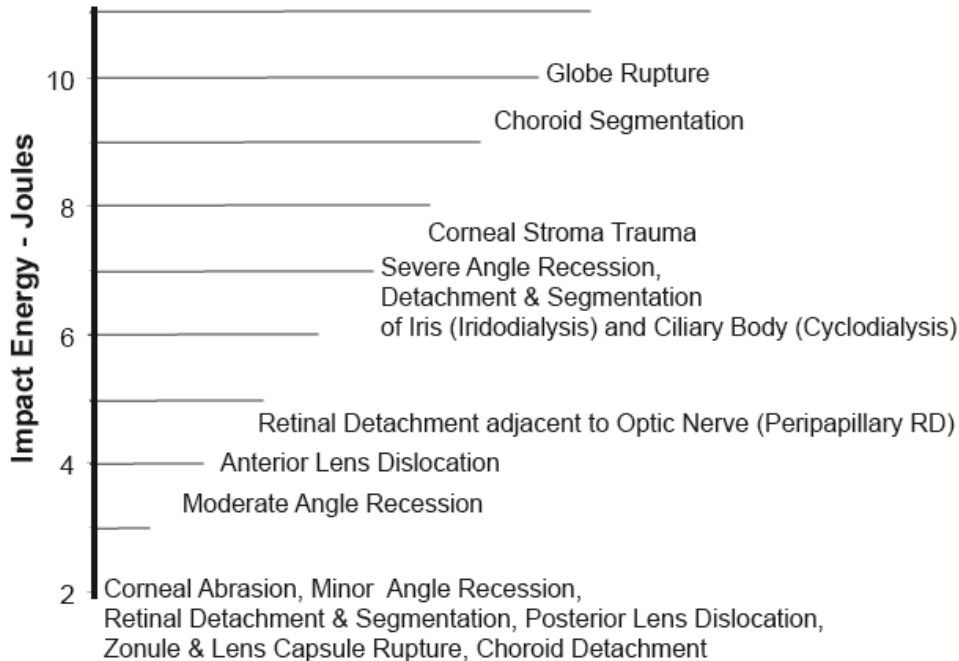


Figure 1. Qualitative trauma thresholds showing lowest energy level for which pathologic entities were observed. Trauma entities were obtained from results of a paintball blunt impact study on porcine eyes (Gray et al., 2008a; Sponsel et al., 2011). The plot illustrates the correlation between impact energy and trauma severity.

Similarly, it is expected that blast-induced ocular trauma should be equally well correlated with blast wave impulse (peak pressure and duration) producing the same types or categories of injury. This hypothesis is supported by results from previous whole-body blast trauma studies that generated the so-called Bowen Curves (Bowen et al., 1968). However, impulse can be roughly equated to incident energy (energy transmitted by the blast wave to the eye) through the relationship:

$$E = \frac{(iA)^2}{2m} \quad (1)$$

where i is the specific impulse (Pa-s) on the exposed area of the eye (A), and m is the mass of the eye specimen. In theory, characterization in terms of incident energy should allow for correlation of injury thresholds observed in primary blast studies with those previously observed in blunt impact studies (Figure 2).

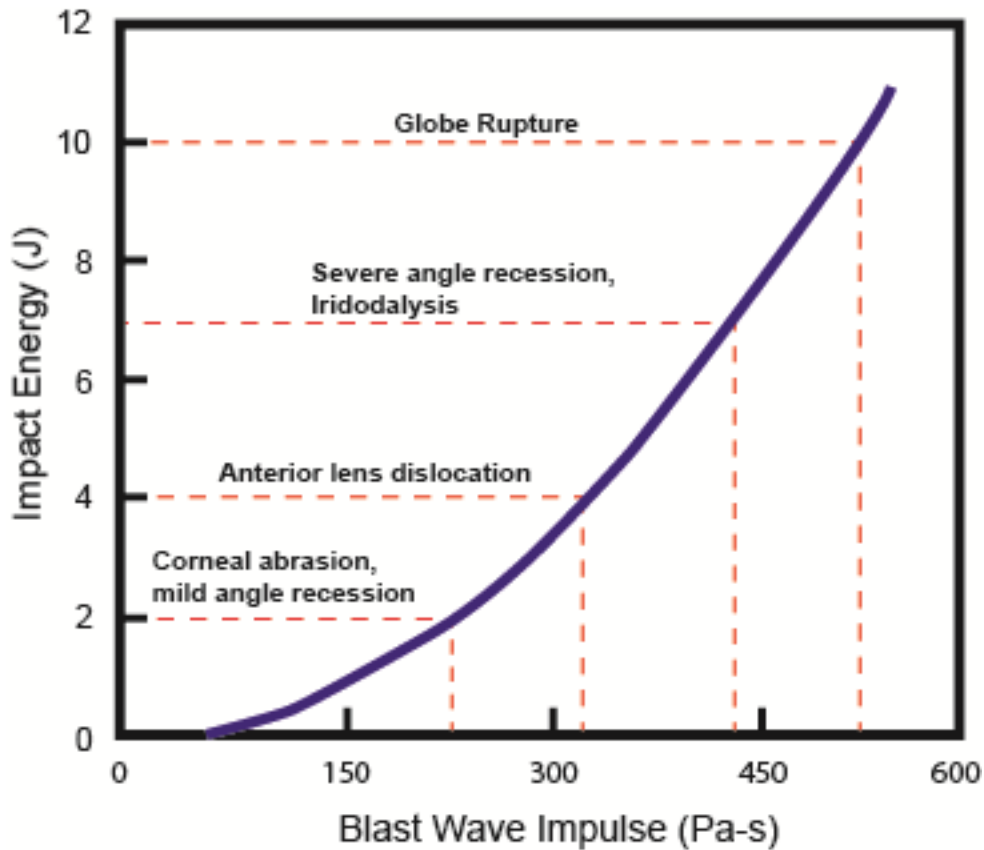


Figure 2. Plot showing hypothesized correlation between impact energy and blast wave impulse. Superimposed on the plot are the observed trauma thresholds from Figure 1 (paintball blunt impact study).

Although globe rupture has been used as the injury criterion in a number of previous blunt impact studies (Kennedy et al., 2004; Duma et al., 2005; Kennedy et al., 2006) the energy required to rupture the sclera is large (~ 9 to 10 J) compared to energy thresholds for less catastrophic but potentially serious injuries to the eye's soft inner tissues (Thach et al., 1999; Sponsel et al., 2011). These injuries typically require immediate surgery and numerous follow-up surgeries to prevent immediate or eventual loss of vision. Thach et al. (2008) estimated that approximately 45% of recent combat eye injuries are closed-globe-type injuries. Recent studies by Duma and Kennedy (2011) and Gray et al. (2008a) characterized closed globe injuries to eyes subjected to projectile blunt impact, but to date no such study has been conducted for primary blast. Thus there exists a significant gap in our knowledge of primary blast effects on the eye, especially internal injuries that occur in the non-lethal or sub-globe-rupture pressure regime.

The primary objective of this research effort is to address this knowledge gap by experimentally identifying sub-globe rupture injury mechanisms and their progression with increasing blast energy and impulse. Blast experiments are being conducted using

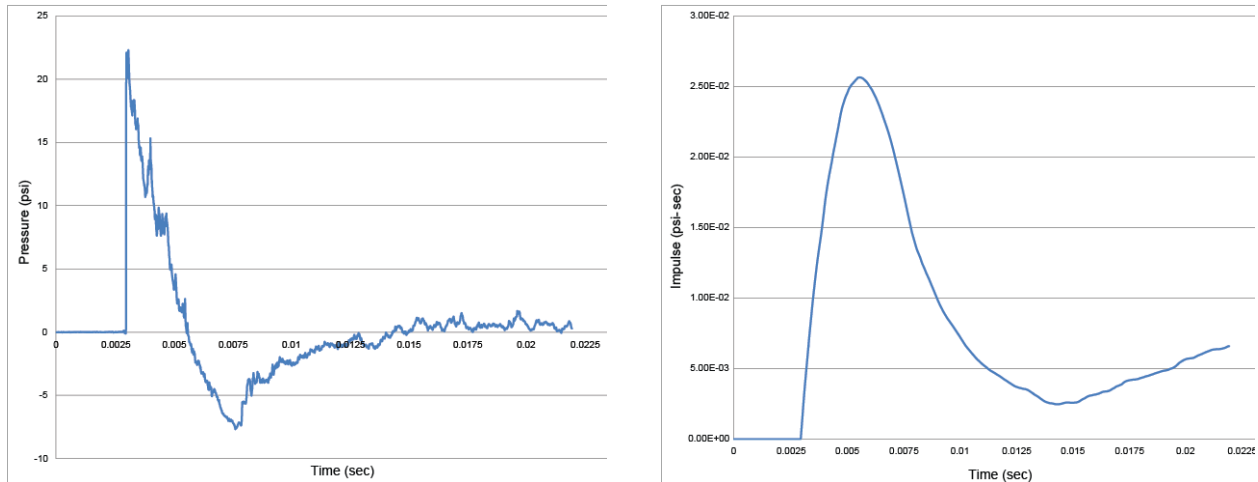


Figure 3. Typical Friedlander waveform (left) and specific impulse (right) for ISR shock tube apparatus. Specific impulse is calculated by time integration of the waveform.

the U.S. Army Institute of Surgical Research (ISR) large diameter shock tube. This device has the capability to reliably produce blast overpressure with the characteristic Friedlander waveform typical of explosive detonation (Figure 3). Integration of the measured pressure-time traces provides the required impulse information. Experiments increase in complexity from *ex vivo* porcine eyes in Year 1 of the study to *in vivo* rabbit eyes in Year 2. Use of the *in vivo* rabbit model will allow for biochemical marker monitoring and characterization. Although physical trauma is the primary focus, the chemical biomarker assessment in Year 2 will allow correlation of observed physical trauma with more subtle chemical indicators.

In addition to ocular trauma, it is anticipated that results of the biomarker study will provide fruitful pathways and directions for future research aimed at understanding blast-induced traumatic brain injury, its recognition, and early treatment. The general approach being taken is a systematic investigation to determine if biomarkers associated with TBI are also present in the experimental animals with blast-induced ocular trauma. The presence of the biomarkers will be probed in samples of aqueous and vitreous humor, as well as blood. All of the protein biomarkers of interest can be measured using Luminex-based, xMAP multiplexed assay panels. Typically 30 microliters or less (sometimes as little as 10 microliters) of sample are required for each multiplexed assay, so this method is very well suited for the limited sample volumes available of ocular fluids. Ocular fluids can be sampled with minimal disturbance to the eye, enabling serial sampling over the course of the study. If the selected biomarkers are present in the ocular and/or serum samples, their amounts will be measured by xMAP assay in eyes subjected to increasing levels of standardized impact severity (as established in the other aims of this research program) to determine if a correlation between biomarker amounts and injury severity exists. The time course of biomarker appearance after injury onset will be characterized. The correlation of the biomarker in the ocular samples with the circulating (serum) levels will also be determined.

In addition to the use of the commercial xMAP bead-based assays, we are exploring the use of Matrix Assisted Laser Desorption Ionization (MALDI), an “imaging” technique for direct detection of protein *in situ*, particularly in optic nerve specimens. This methodology not only determines the sequence of proteins or protein fragments, but also identifies the spatial localization of proteins in a tissue sample. A section of the tissue is prepared for the laser assisted matrix desorption process, then the activating laser is stepped across the tissue in a raster pattern. The intensity of the ejected ions (specifically, the mass/charge or m/z ratio) is plotted as a function of the position of the laser beam on the tissue. The map of ion location produces an “image”, thus mapping the location of the protein being analyzed. This approach may be particularly productive in analyzing biomarkers in optic nerve sections taken from traumatized eyes.

Experiments are accompanied by computational analysis using physics-based codes CTH and LS-DYNA. One of the invaluable lessons learned in previous blunt impact studies was that numerical simulations have the potential to identify physical mechanisms responsible for otherwise unobservable and unexplained phenomena (Gray et al., 2008a, 2011). Realistic geometrical and tissue constitutive models of external and internal eye structures are being developed for implementation into CTH and LS-DYNA. Co-development of models for both codes allows us to avoid limitations presented by each code. The objective here is to use CTH in the initial stages of the shock interaction (i.e., the first few μ sec), where it can produce the initial boundary condition inputs for LS-DYNA. LS-DYNA will be then be used to simulate long-term deformation (msec to sec). The simulations carefully mimic the experiments with the goal of fully reproducing the trauma observed in the experiments. The validated models will allow for analytical extension into impulse regions unattainable with the shock tube experiments. The models will be invaluable in characterizing the physics of tissue response, design of protective eyewear, and virtual measurement of physical parameters not measurable in the experiments.

Extensive use of *in situ* imaging technologies is being employed for pre- and post-blast assessments. In-house studies of impact trauma have shown that pre- and post-impact B-scan and UBM ultrasound imaging help differentiate blast-induced trauma from fixative artifact. Scanning abattoir eyes from a posterior approach allows cilio-lenticular imaging with B-scan, and peripapillary/macular assessment with UBM, greatly increasing the diagnostic specificity of the histopathology studies. Gross globe deformation that occurs during the blast will be documented using bidirectional high-speed digital video.

The project will culminate in Year 3 with development of trauma predictive models. The data generated during the experiments will be used to formulate empirical models useful in predicting the probability of observing a number of sub-globe-rupture injuries under various blast pressure-impulse or energy environments. We envision that the model will consist of a series of curves in peak pressure-impulse space, similar in form to those used to predict whole-body response to blast (Richmond and White, 1962; Richmond et al., 1966; Bowen et al., 1968; Richmond, et al., 1985; Proud et al., 2009). The utility of such models has been adequately demonstrated by the wide use of

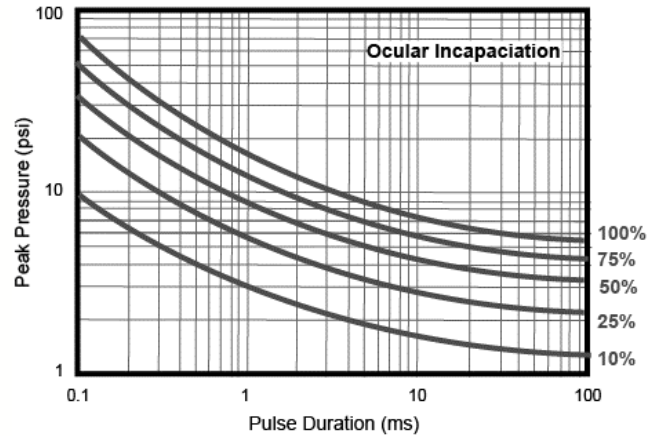
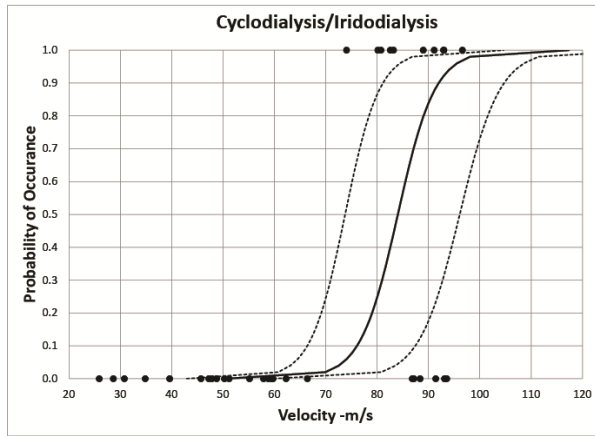


Figure 4. Probability of injury curve (risk function curve) for projectile blunt impact (left). Example of proposed ocular incapacitation chart based on medical assessment of the overall impact of cumulative ocular injuries on the warfighters ability to carry out his mission (right).

Bowen-type curves (whole body response to blast) in a number of warfighter survivability, lethality, and vulnerability (SLV) models. Individual curves will reflect the probabilities of observing such injuries as angle recession, iridodialysis/cyclodialysis, scleral rupture, etc (Figure 4). In addition to physical injury curves, medical assessments will be performed on the individual injuries and combinations of injuries to develop qualitative curves detailing level of soldier ocular incapacitation (as a function of the blast pressure-impulse condition), typically a more useful tool for first responders and warfighters (Figure 4).

2. SUMMARY OF RESEARCH

2.1 Blast Experiments

A total of 68 blast experiments on abattoir porcine eye specimens have been conducted to date at peak blast overpressures of approximately 28, 48, 96, 131, and 152 kPa (with repeats) in accordance with the test plan (Appendix I). All blast experiments were conducted at the ISR Shock Tube Laboratory (STL) located at Joint Base San Antonio, San Antonio, TX. The 68 experiments represent approximately 80% of the porcine experiments planned for year 1 as outline in the test matrix (Table 1). Our original intent was to conduct blast testing at two different shock tube driver volumes (defined in the test matrix as driver volumes 1 and 2). The driver volume controls the amount of high-pressure air available in the shock tube during creation of the blast wave. The biggest effect of changing the air volume is an increase in the pulse width or duration of the shock profile. By increasing the driver volume we had hoped to increase the pulse width, thus increase the total impulse and energy of the blast wave. However, during preliminary trials with the increased volume (~ 16x), damage occurred to the shock tube laboratory facility as well as to some associated

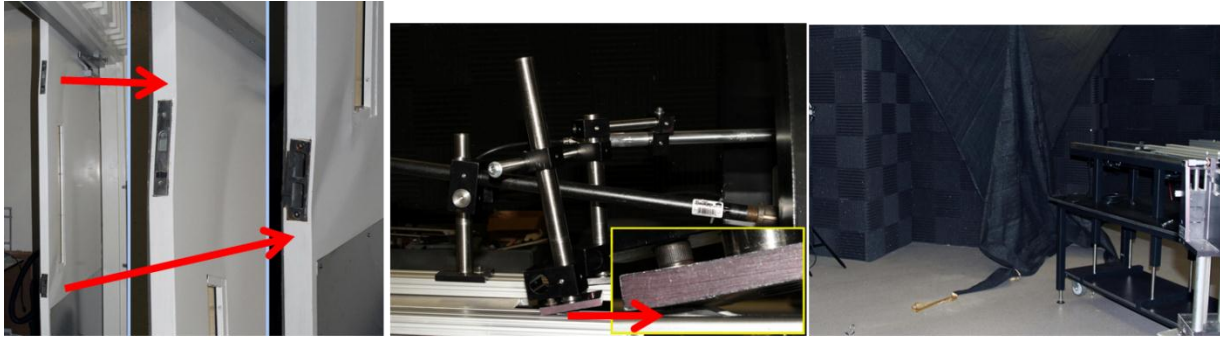


Figure 5. Damage to the Shock Tube Laboratory and equipment due to blast at full driver volume. Left: damage to the blast doors. Center: damage to the sensor mounts. Right: Damage to the blast curtain.

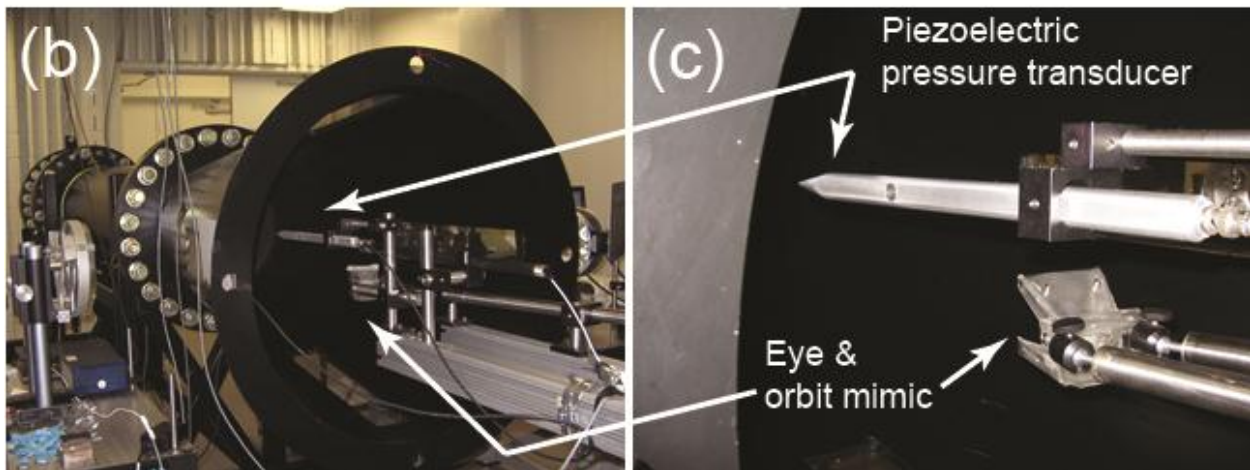
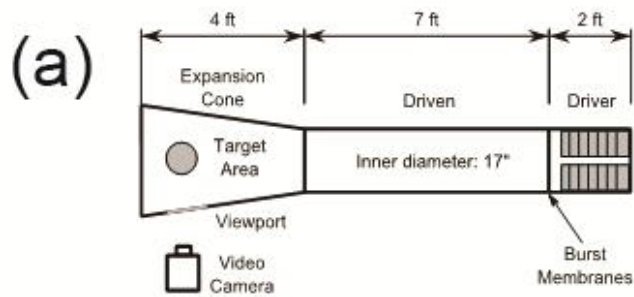


Figure 6. US Army Institute of Surgical Research shock tube showing location and orientation of eye and holder (orbit mimic) along with piezoelectric pressure transducer. A shock wave is created by pressurizing the driver section until the burst membranes ruptures. The target area lies within the expansion cone. Exposures of the pig eyes were recorded using an ultra-high speed video camera looking through an open viewport on the side of the expansion cone.

instrumentation (Figure 5). The damage has now been repaired, but it resulted in a delay in the test schedule. However, it is now clear that we will not be able to conduct tests at the increased driver volume as originally planned. We are now considering what other volumes or test conditions we want to pursue.

2.2 Shock Tube

Blast exposure testing at the STL was accomplished using a 17-inch diameter compressed air driven shock tube (Figure 6). The eye specimen and acrylic holder (orbit mimic) were placed within the expansion cone of the shock tube and isolated from the driver section by a series of thin (.016 inch thick) aluminum disks. Pressurization of the driver section causes the disks to rupture, sending a Friedlander-style pressure wave down the tube toward the eye specimen. The peak pressure of the shock wave is controlled by the number of disks. Experiments have been performed using from 1 to 6 aluminum disks resulting in peak pressures from approximately 48 kPa (7 psi) to 152 kPa (22 psi). In addition, experiments have been conducted at a pressure levels lower than 48 kPa by using a 0.007-inch thick mylar disk. Peak pressures up to 35 psi (241 kPa) were achieved by moving the eye-orbit mimic further axially into the expansion cone, while peak pressures as low as 3 psi (21 kPa) were achieved using a single 0.010-inch thick mylar disk.

Each blast experiment was documented using high-speed videography at 15,000 frames/second using a Fastcam Ultima APX (Photron USA, Inc; San Diego, California). Blast overpressure (static or side-on pressure) was recorded using piezoelectric pressure transducers (Model 137A23; PCB Piezotronics, Inc; Depew, New York). Stagnation pressure (reflected pressure) was recorded with a Kulite pressure transducer (Model XTL-190; Kulite Semiconductor Products; Leonia, New Jersey) as shown in Figure 7. Both pressure probes were factory calibrated with appropriate certificates of conformance provided by the manufacturer. Pressure signals were recorded at 200,000 samples per second using a Synergy P Data Acquisition System (Hi-Techniques, Inc.; Madison, Wisconsin). The pulse duration of each experiment was taken as the point where the initially positive phase of the wave form reaches zero pressure, i.e., the negative phase of the waveform is ignored (Figure 3). The specific impulse is calculated by time-wise integration of the entire waveform.

In its original configuration, the volume of the driver section (where high pressure air is injected and stored prior to disk rupture) is approximately 170 in³ (Figure 8). This volume of air provides consistent positive pulse durations of approximately 2 ms. However at this impulse level, trauma to the eyes has generally been lower than anticipated resulting in a sparse number of positive trauma observations (see Section 2.6). In an attempt to alleviate this difficulty, we removed all of the several metal plates in the driver section volume in an attempt to increase the pulse width to approximately

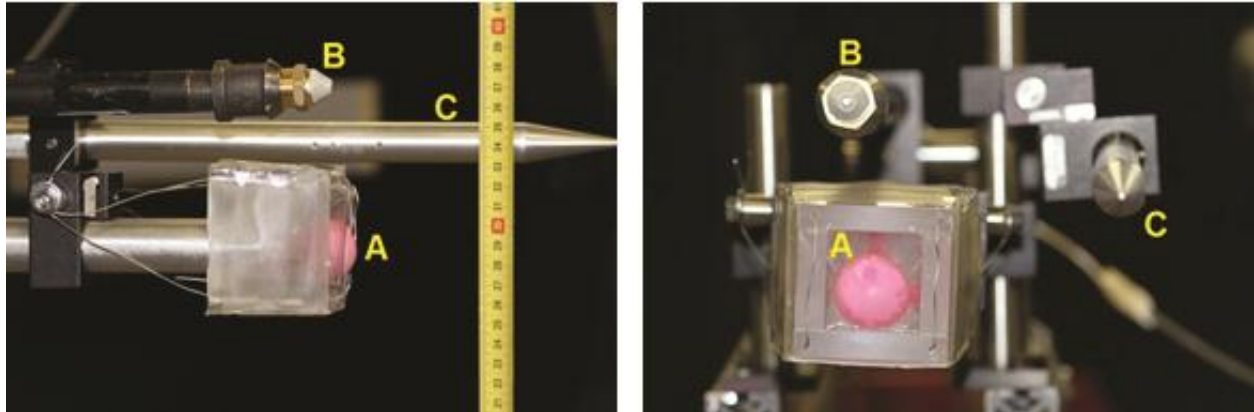


Figure 7. Arrangement of target and pressure sensors used to investigate physical effects of primary blast waves on the eye. A) Water-filled balloon (as substitute for eye) embedded in gelatin, and mounted in acrylic eye socket mimic. B) Pressure sensor to measure total pressure. (Kulite XTL-190 pressure transducer) C) Pressure sensor to measure overpressure (PCB Piezoelectronics Model 137A23 ICP Blast Pressure Sensor).

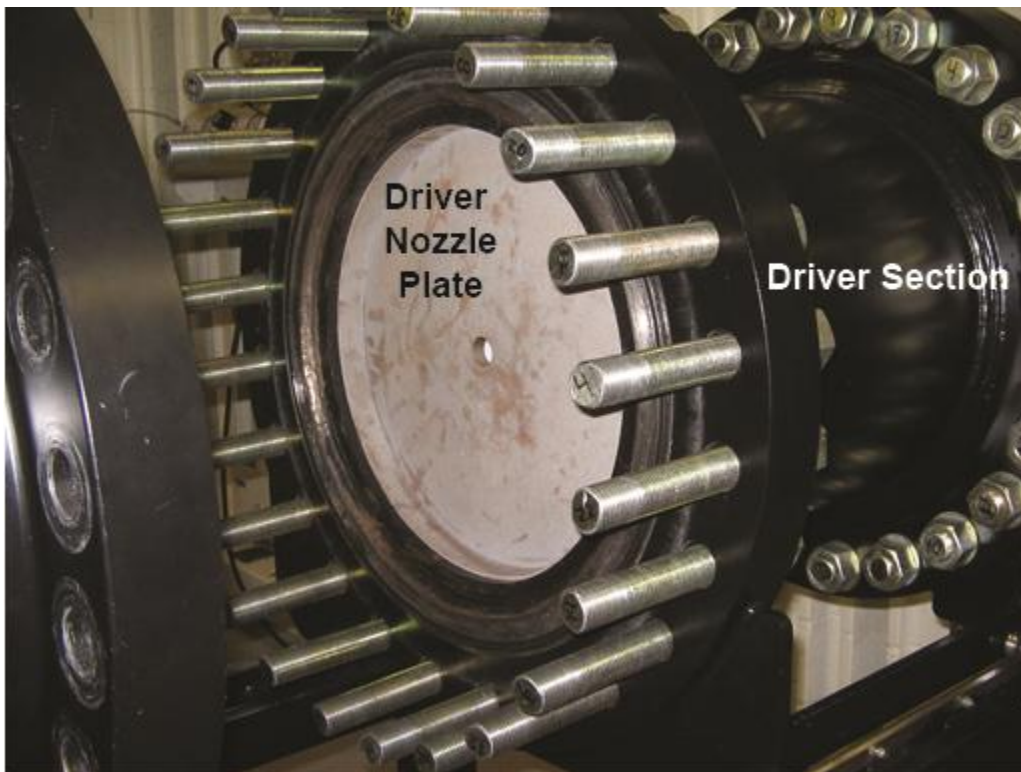


Figure 8. Metal plates located behind the driver nozzle plate can be removed to increase the volume of high pressure air stored in the driver section. In theory this should increase the Friedlander waveform pulse width from 2 ms to approximately 4 ms. However, during initial trials, damage occurred to the shock tube facility as well as associated equipment and instrumentation.

3.5 to 4 ms. In theory this would increase the energy content of the Friedlander waveform and, in turn, the exposure trauma. Unfortunately, during preliminary testing with the larger driver volume, damage occurred to the shock tube facility as well as to associated equipment and instrumentation. Thus it is clear than testing with the full driver volume (all plates removed) is not possible. We are currently pursuing alternatives to this approach.

2.3 Porcine Eye Specimen Preparation

Porcine eyes, including eyelids and extraocular muscles, were purchased from Animal Technologies, Inc. (Tyler, Texas) and shipped overnight on wet ice. All animal tissues were handled in accordance with the ARVO Statement for the Use of Animals in Ophthalmic and Visual Research and protocols approved at each institution. The superior sclera was first marked using a surgical marker based on eyelid position to allow repeatable identification of locations on each eye. Skin, muscles, eyelids, and fatty tissues were removed to expose the surface of the globe, then placed in Hanks Balanced Salt Solution (HBSS; Fisher Scientific; Hampton, New Hampshire) and transported to the pathology laboratory.

Despite transfer on ice, the hydraulic conductivity of the scleral membrane and the necrotic state of the tissue, rendered the initial the intraocular pressure (IOP) of the porcine eyes low. Evidence for this was the observed flaccid cornea, soft eyewall, and failed readings from our Tono-Pen VET (Dan Scott & Associates; Westerville, Ohio). It was often necessary to re-inflate the porcine eyes to a normal level (10-20 mmHg) with HBSS before scanning and blast testing. We found that injections at the pars plana increased the fluid content of the posterior chamber, allowing subsequent anterior chamber injections to maintain a normal IOP. At the pathology laboratory, each eye was re-inflated via pars plana injection of HBSS using a 30 gauge needle until the IOP was between 10-20 mmHg as determined by the Tono-Pen. B-scan (Compact Touch; Quantel Medical; Bozeman, Montana) and ultrasound biomicroscopy (UBM; OIS-100; i-Science Interventional; Menlo Park, CA) were used to assess the condition of each pressurized eye prior to blast exposure. B-scans were taken from 3 to 9 o'clock, 6 to 12 o'clock, and 9 to 3 o'clock axially and posterior near the optic nerve to visualize the anterior chamber. UBM was used to image each eye from pars plana, equator, and peripapillary regions from clock hours 12, 3, 6, and 9. Eyes were rejected from the study if pre-exposure pathology was observed during this pre-screening process. After screening, eyes were stored refrigerated (4°C) overnight in HBSS then transported to the shock tube laboratory. Several acrylic orbital mimics were fabricated with internal dimensions and geometry similar to the orbital structure (Sponsel et al., 2011; Kennedy et al., 2007; Weaver et al., 2010). A plastic cup with spherical bottom (diameter roughly equivalent to the porcine globe) was placed in the center of the orbit mimic and the remaining internal volume filled with a liquid gelatin mixture (Knox Gelatin; Kraft Foods; New York, New York) which was cooled overnight prior to delivery of the eyes (Figure 9a). This gelatin has been shown to provide nearly equivalent mechanical strength as the extraocular muscles and the associated periorbita (Kennedy and Duma, 2008).

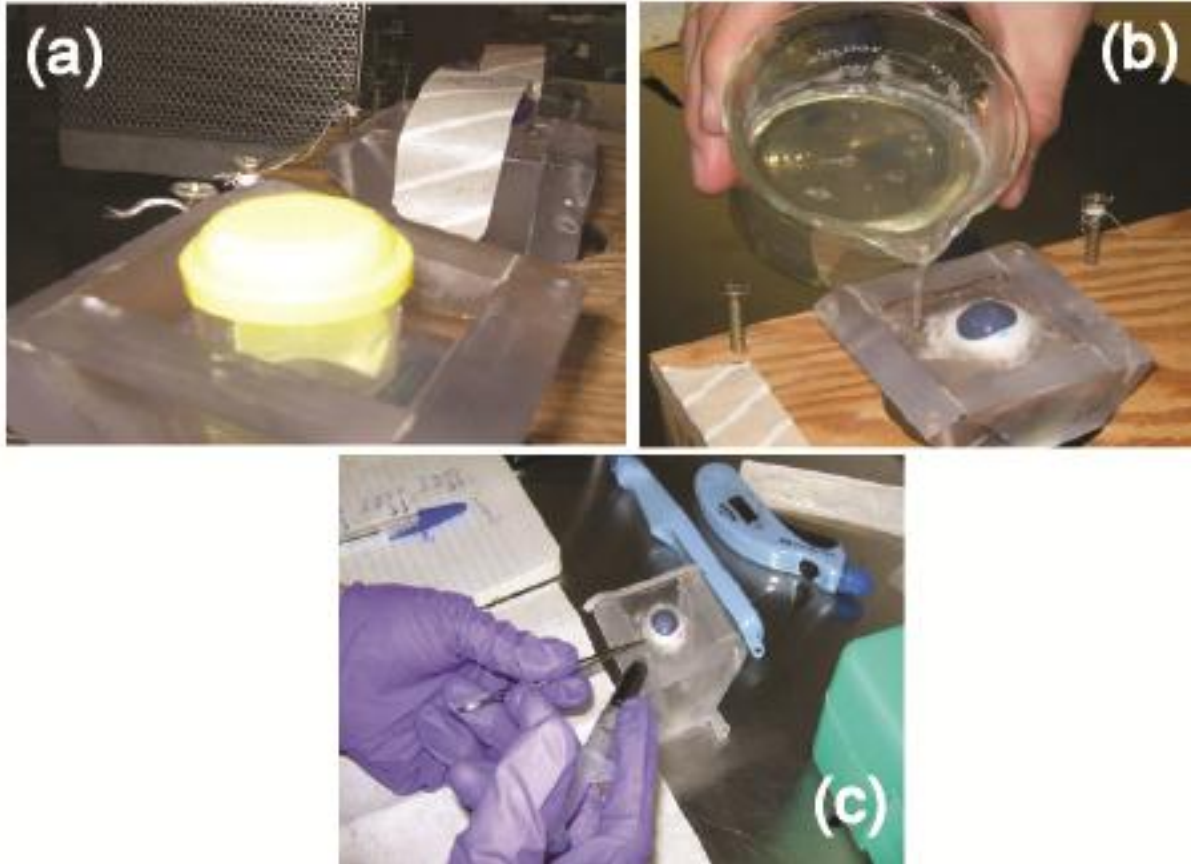


Figure 9. (A) Gelatin is preformed into acrylic holders that simulate the interior dimensions of the orbit. (B) Eyes are oriented and set within the preformed gelatin and sealed in place. (C) Just prior to blast testing, HBSS is injected in to the anterior chamber at the pars plana. The needle is inserted nearly parallel to the corneal surface in an attempt to provide for some degree of self-sealing once the intraocular pressure is raised.

Each eye was re-inflated via pars plana injection with HBSS and set in place of the plastic cup within the gelatin. Additional liquid gelatin was then poured around the eye filling the holder to the top (Figure 9b). The eye and orbit mimic was then refrigerated for approximately 30 minutes to fully set the gelatin. During refrigeration, each eye was covered with parafilm to prevent dehydration of the specimen.

Just prior to blast exposure HBSS was injected into the anterior chamber via a shallow angle through a 30-gauge needleport paracentesis tangential to the limbus in the peripheral cornea (Figure 9c). The eye-orbit mimic assembly was then photographed and placed into a rigid mount inside the shock tube. Once secured, the IOP was measured again and recorded. The eye-orbit mimic was tilted 20 degrees laterally to simulate the convergence of the human eye and placed 25 cm into the expansion cone of the shock tube. The test chamber was cleared, the driver section of the shock tube pressurized, and the blast test conducted.

For each day of testing, this procedure was repeated for several exposed eyes and one control eye. The control eye was treated in an identical fashion to the test eyes, i.e., placed into the expansion cone for several minutes but never subjected to an actual overpressure. After the test, IOP was measured and recorded; the eye-holder assembly was removed from the rigid mount, and another series of photographs taken. The eye specimen was then removed from the gelatin and placed into a HBSS-filled container. The containers were then transported in small plastic containers on ice to the pathology laboratory for blind post-test damage assessment.

Upon arrival at the pathology laboratory, another corneal HBSS injection was used to raise the IOP to between 10-20 mmHg through a 30-gauge needleport paracentesis tangential to the limbus. Trauma damage to each eye was then evaluated and documented using a combination of B-Scan and UBM ultrasound imaging along the meridians and directions examined previously. The severity of injury was estimated via cumulative injury algorithm by an eye trauma surgeon at William E. Sponsel Associates (WES) using a weighted scale where 0 represents no injury, 1 a minor injury (potentially self-correcting *in vivo* without surgery), 2 a significant injury (likely to require surgical repair to sustain visual function), 3 a debilitating injury (potential for severe sustained visual loss despite successful surgery), and 4 a catastrophic injury (unlikely to yield useful visual function even with extensive surgery). Separate scores were rendered for the sclera, chorioretina (composite), retina, choroid, and peripapillary zone. The specimens were then placed in formalin in preparation for detailed examination via manual dissection (in which the anterior surface was removed with a diamond knife) or histological analysis. Anterior chamber and optic nerve status were further assessed via stained paraffin sections of a subset of specimen eyes representing controls and the full primary blast testing range. A total of 60 eyes were treated in this way. Thirteen (13) were used as controls while the balance (47) were exposed to primary blast. Additional eyes were used in preliminary testing to develop the methods described above. Specifically, with these additional eyes we determined that placing control eyes in formalin prior to the post-ultrasound examination introduced artifacts in nearly every control eye. We also found that failing to re-inflate the eye prior to blasting resulted in much more extensive damage than that observed in eyes with physiological IOP values. Another 10% of eyes received for study were excluded because the B-scan and UBM ultrasonic pre-screening demonstrated the presence of pre-existing damage to the eye.

Linear regression was used to determine whether injury scores were significantly correlated with the peak overpressure, duration, or specific impulse of the shock wave. Regression for each of the three zones specified in the Ocular Trauma Scoring System (OTCS, Pieramici et al., 1997) utilized scores that were taken as the sum of trauma scores for all tissues within that zone (e.g. an eye with retinal trauma scored as 3, choroid trauma as 1, and lamina cribrosa as 2 would be scored with a 6 for zone 3).

2.4 Pathology

Using terminology consistent with the OTCS (Pieramici et al., 1997), the majority of ocular injuries resulting from blast exposure were found to be lamellar injuries. Probability of injury was found to increase with peak overpressure in Zone 1 (external surface; $p=0.024$) and Zone 3 (internal posterior segment; $p=0.023$) while no significant correlation was found in Zone 2 ($p=0.6242$). Injuries included angle recession, cyclodialysis, peripheral chorioretinal detachments, radial peripapillary retinal detachments, and internal scleral delamination. No full-thickness openings of the eyewall (scleral rupture) were observed in any of the eyes tested. A summary of preparation and exposure information for the 60 eyes is provided in Appendix II. The peak pressure was not independent of the duration of the positive phase: as the peak pressure increased, the duration increased as well (Figure 10). Any type or level of trauma observed in the subject area (i.e., angle, choroid, etc.) is reported in that category regardless of the severity. Corneal abrasion was ubiquitously observed in exposed eyes and so was not counted in the linear regression analysis. Macroscopic injury of the iris and anterior chamber occurred infrequently and was generally restricted to the angle. The increase in severity and occurrence of injury did not appear to be a deterministic event, but the results support the idea that certain ocular tissues are more sensitive to increases in blast energy than others. The retina appears to be the very sensitive to increasing blast energy. The sclera demonstrated the strongest associative tendency for increasing injury with increased overpressure (Figure 11). Remarkably, at very high levels of overpressure (>300 Pa-s) the injury quotient for the sclera and the various other ocular tissues tested returned to control eye values. Angle injuries also showed a bell-curve response, with injuries beginning to appear at the 50 Pa-s level and tapering back to baseline at 200 Pa-s. There was no obvious impulse threshold value for the appearance of lower-grade injury to any ocular structure, but there were such thresholds in evidence for more extreme damage levels readily apparent for the optic nerve (~ 125 Pa-s), anterior chamber (~ 100 Pa-s), and sclera (~ 90 Pa-s; Figure 12).

Pathology– Zone 1: Scleral delamination and multiple chorioretinal detachments were observed before fixation using B-scan and UBM, and were confirmed through dissection and histopathology. Figure 11a shows a chorioretinal delamination following exposure to 138 kPa (20 psi) blast. Figure 11b shows a detachment in an eye that was exposed to 113 kPa (16 psi) blast. These lamellar lacerations occurred in multiple meridians. UBM scans also showed significant chorioretinal disruption with the probe oriented equatorially (Figure 13a) and with probe oriented postero-anteriorly (Figure 13b) following exposure to 38 kPa (5.5 psi) blast. One of the strengths of using UBM was the ability to place the probe in the same location before and after blast testing. Figure 14 shows three eyes exposed to three different peak pressures. Figure 14b shows an eye exposed to a peak pressure of 152 kPa, which caused significant delamination of the chorioretina. Figure 14c shows an eye that was exposed to a peak pressure of 134 kPa. Figure 14f shows an eye that was exposed to a peak pressure of 126 kPa, which caused the retina to detach and crumple.

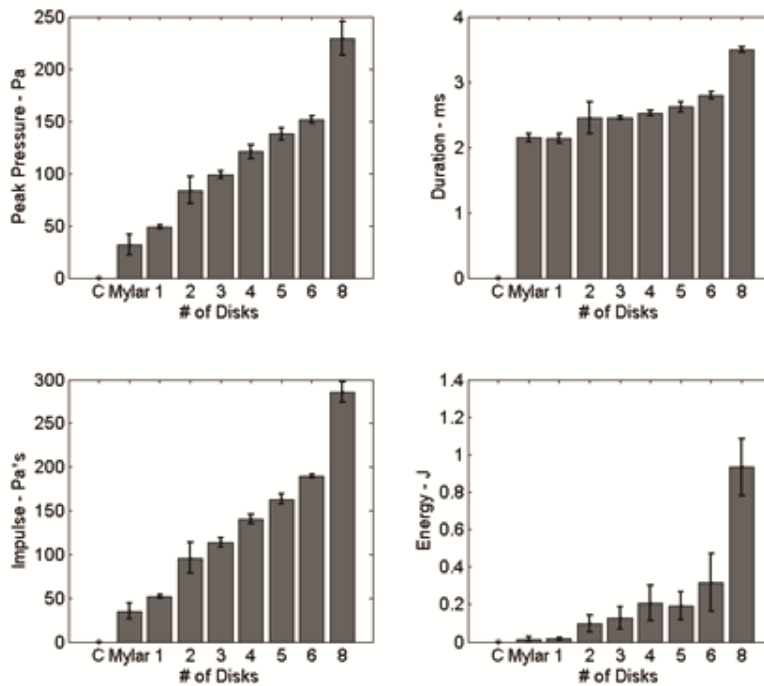


Figure 10. Histogrammic representation of the association of the number of mylar or aluminum disks secured between the pressure chamber and shock tube and peak pressure (upper left), duration (upper right), impulse (lower left), and energy (lower right)

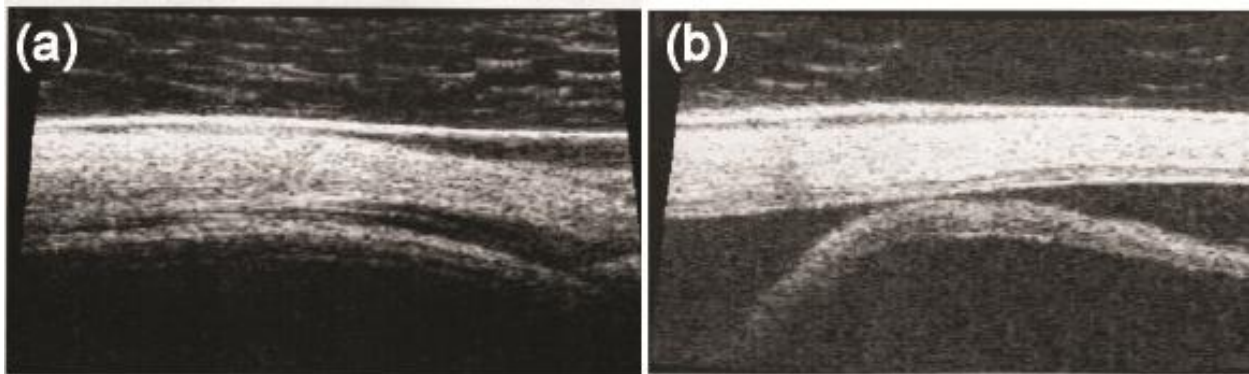


Figure 11. Scleral delamination and multiple chorioretinal detachments were observed before fixation using B-scan and UBM, and were confirmed through dissection and histopathology. Scleral delamination (a) following exposure to a 138 kPa (20 psi) blast, and extensive chorioretinal detachment (b) in eye exposed to a 113 kPa (16 psi) blast.

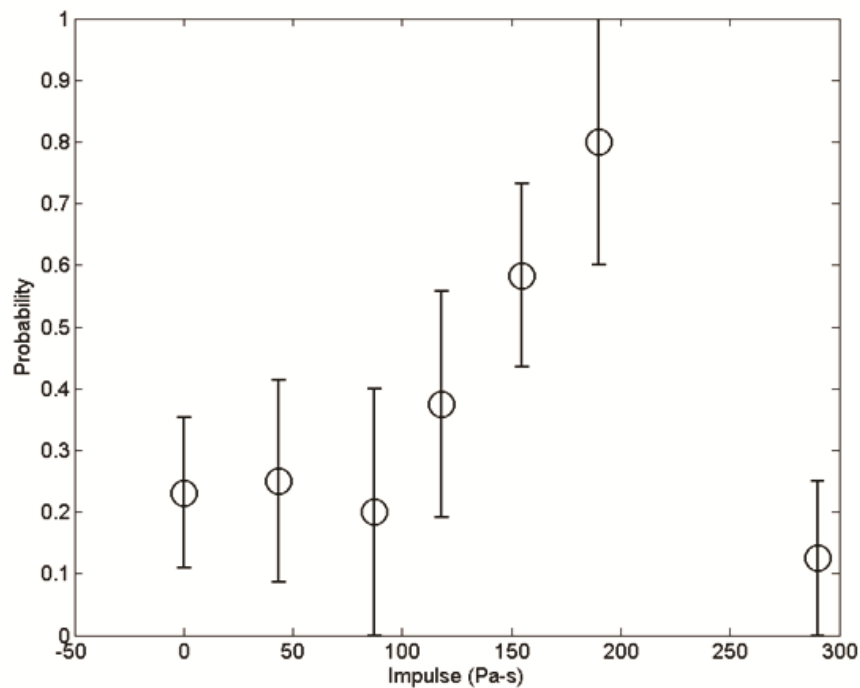


Figure 12. Histogram showing the probability of scleral injury for a given impulse level. Delamination accounted for nearly all observed scleral trauma. Note that the likelihood of injury increased to around 200 kPa (29 psi) above which the probability returned to that of the controls. While the exact mechanism underlying this observation is unknown, similar probability peaks have been observed in other ocular tissues within the present study. A numerical model of the blast may elucidate the underlying cause of this counterintuitive finding.

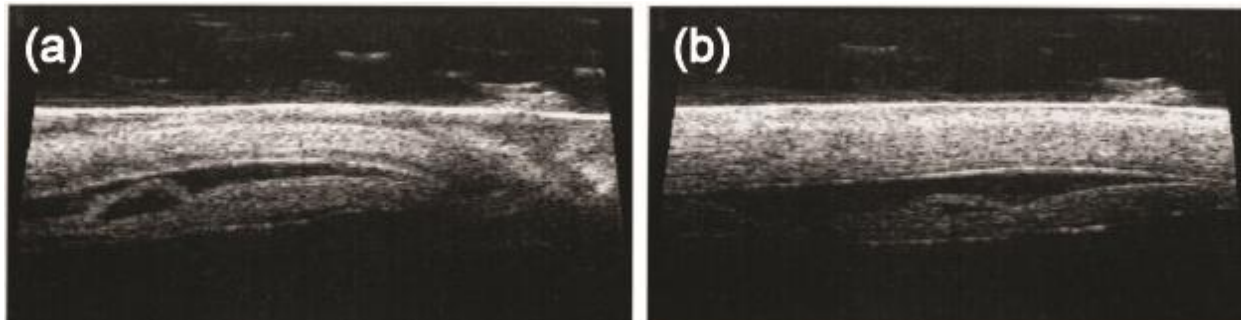


Figure 13. UBM shows significant chorioretinal disruption with probe oriented equatorially (a) and postero-anteriorly (b) following exposure to a 38 kPa (5.5 psi) blast.

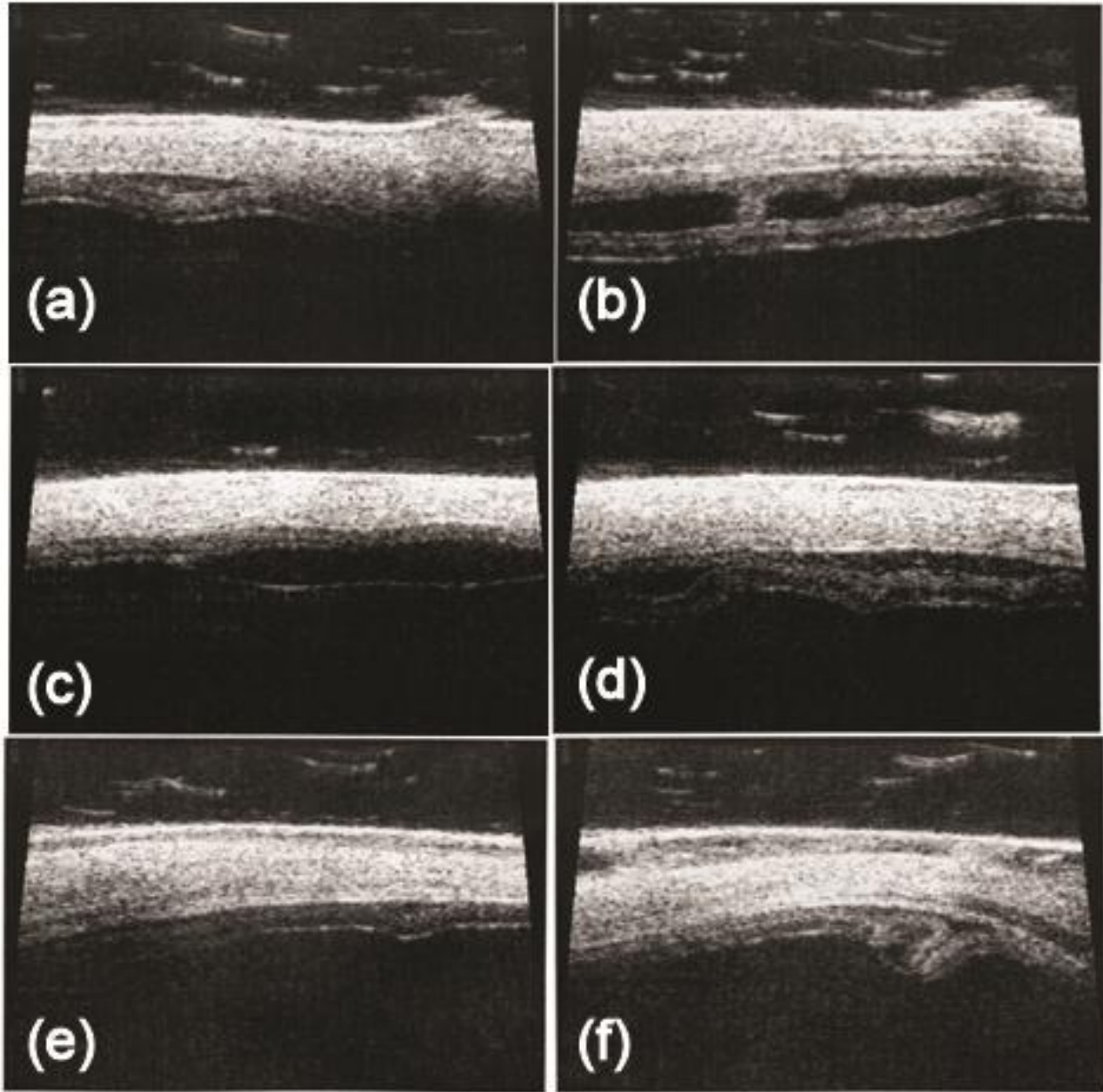


Figure 14. UBM scans of eyes exposed to three different peak pressures showing typical delamination injuries observed after blast exposure. (b) severe delamination of the chorioretina after exposure to a peak pressure of 152 kPa, (c) similar but less severe injury after exposure to a peak pressure of 134 kPa, and (f) detachment and crumpling of retina after exposure to peak pressure of 126 kPa.

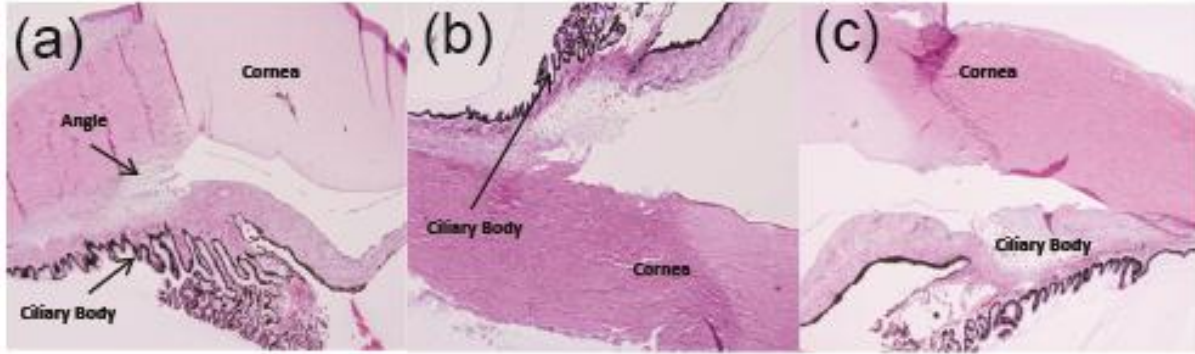


Figure 15. Histopathology of the porcine eye angle in (a) a control eye, (b and c) eyes exposed to 113 kPa (16 psi) blasts. Both angle recession (b) and cyclodialysis (c) were observed. Significant damage to the angle was commonly observed even after low peak overpressure exposures.

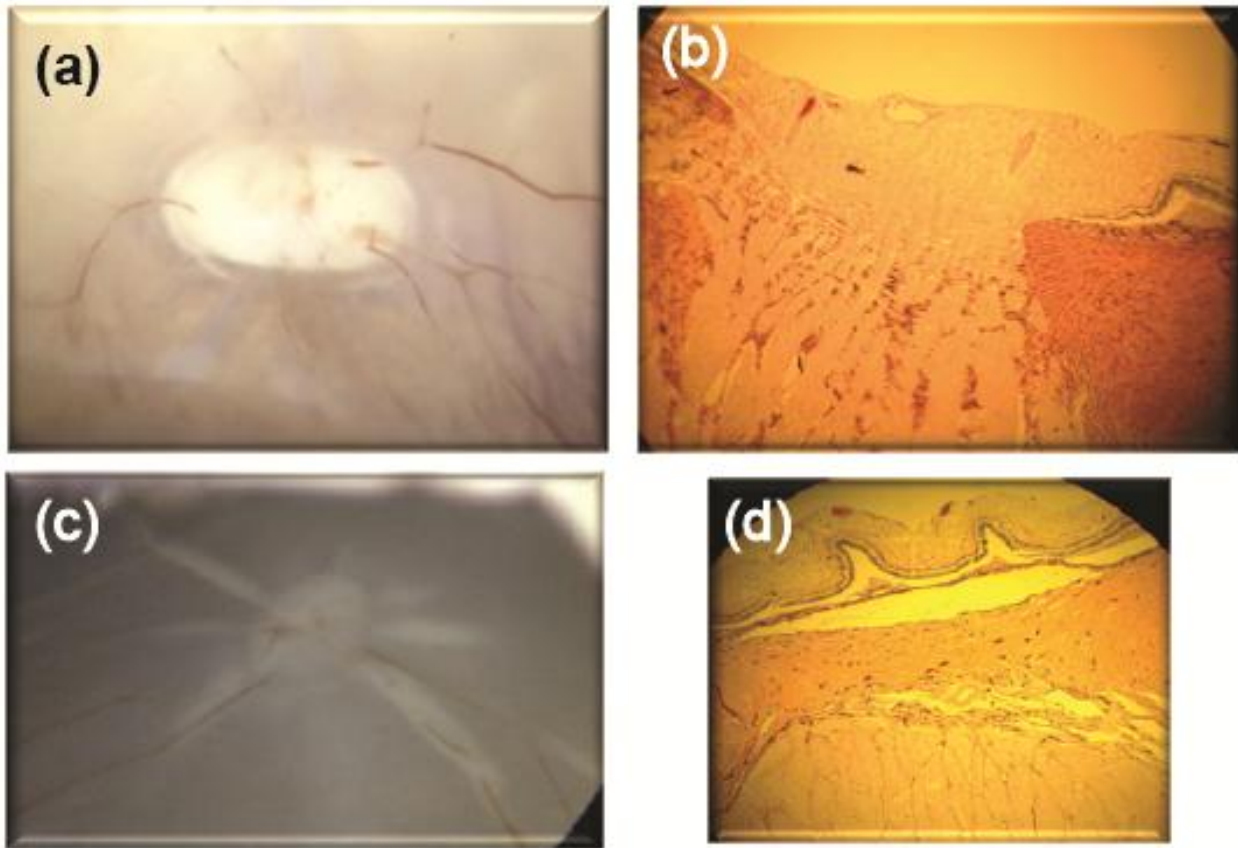


Figure 16. Images of the optic nerve head (ONH) taken during manual dissection (above) and from histopathology (below). (a) Control eye showing clear ONH as viewed through the vitreous after removal of the anterior chamber. (b) Eye exposed to 207 kPa (30 psi) blast shows retinal elevations coinciding with the location of blood vessels originating from ONH as viewed through the vitreous after removal of the anterior chamber. (c) Control eye section shows normal ONH and surrounding tissues. (d) Eye exposed to 126 kPa (18 psi) blast shows retinal folding in the immediate vicinity of blood vessels. Such injuries may be due to rapid oscillations in the tissue following blast exposure and may induce large strains in the region of density gradients such as at the blood vessel-retina interface.

Pathology– Zone 2: Angle obliteration was observed via histopathology after the eye was exposed to peak overpressure of 113 kPa (16 psi; Figure 15). UBM was generally unable to resolve this injury. However, histopathology revealed the angle as a common location for injury, even for porcine eyes exposed to low peak overpressures

Pathology– Zone 3: Images of the optic nerve head (ONH) were taken during manual dissection and from histopathology (Figure 16). The ONH of the control eye was normal when viewed through the vitreous after removal of the anterior chamber. The ONH of an eye exposed to a 207 kPa (30 psi) blast showed retinal elevations coinciding with the location of blood vessels originating from ONH as viewed through the vitreous after removal of the anterior chamber. Examples of such injuries may be due to rapid oscillations in the tissue following blast exposure. Such oscillations could induce large strains in regions with density gradients such as at the blood vessel-retina interface.

2.5 Biomarker Study

In addition to the use of the commercial xMAP, bead-based assays, described in the original proposal for the detection of trauma-associated protein biomarkers, we have also been preparing to use “imaging” MALDI for the direct detection of protein *in situ*, particularly in optic nerve specimens. This technique was not available locally when the proposal was written, but it is coming on-line now at the UTSA, in the Department of Chemistry. This methodology, called MALDI Imaging (Matrix Assisted Laser Desorption Ionization), not only determines the sequence of proteins or protein fragments, but also identifies the spatial localization of proteins in a tissue sample. A section of the tissue is prepared for the laser assisted matrix desorption process, and then the activating laser is stepped across the tissue in a raster pattern. The intensity of the ejected ions (specifically, the mass/charge or m/z ratio) is plotted as a function of the position of the laser beam on the tissue. The map of ion location produces an “image”, thus mapping the location of the protein being analyzed. This approach may be particularly productive in analyzing biomarkers in optic nerve sections taken from traumatized eyes.

To prepare tissue for the MALDI technique, sections were cut from optic nerve specimens collected from eyes subjected to blasts in the shock tube, as well as unexposed, control eyes, which were frozen immediately after the experiment. We have successfully cut 20- μm thick frozen sections from the optic nerve specimens using a cryostat, and mounted these sections on indium titanium oxide (ITO)-coated slides used for MALDI analysis following, in part, a protocol described by Grey et al. (2009). The sections were mounted on the ITO slides from a methanol layer, and appear to have attached well on to the slides after evaporation of the methanol. The slides are currently stored at $-75\text{ }^{\circ}\text{C}$ until time can be arranged on the Bruker MALDI at UTSA. The initial work will be to look for the presence of some of the trauma-related proteins identified in the proposal, as listed in the following table. Proteins will be identified by the homology of the measured m/z spectra with protein sequences published in the UniProt database (Table 1). Software supplied by Bruker will be used for the proteomic

Table 1. Biomarker Protein Sequence Data Obtained from the UniProt database (www.uniprot.org)

Protein biomarker	UniProt ID	# of Amino Acids	Functional Regions
αII-spectrin	P02549	2419	at least 25 identified regions
Tau	P10636	758	4 regions
S100β	P04271	92	4 regions
Glial Fibrillary Acidic Protein	P14136	432	10 regions
Ciliary Neurotropic Factor	P26441	200	regions not identified

identification, as well as to create the graphic representation of the protein abundance and location in the tissue specimens.

In addition to the use of multiplexed, bead-based (Luminex xMAP) immunoaffinity assays an additional, mass spectrometric approach has been adopted for the direct detection of protein in histological sections of retina and optic nerve. The technique, called imaging MALDI, is a variant of Matrix Assisted Laser Desorption Ionization (MALDI), which not only determines in a tissue section the sequence of proteins or protein fragments, from which the identification of the parent proteins may be made, but also identifies the spatial localization of proteins in the tissue sample. The imaging MALDI technique was not available locally when the proposal was written, but the purchase of an instrument by the Department of Chemistry at the University of Texas at San Antonio was realized through the receipt of a Major Research Instrumentation Grant from the National Science Foundation. Through pre-existing collaborative links, the biomarker investigation team of the SLOT project has been able to utilize this instrument. We have now obtained some initial results from both the *ex vivo* porcine ocular tissue, as well as from some pilot studies using cadaver rat eyes. Because these studies have been conducted in *ex vivo* or cadaver eyes, we did not expect to find novel proteins expressed in tissues subjected to blasts; therefore, the purpose of this study was to learn how to apply the method to the ocular samples and, as a form of validation of the technique, to determine if different protein mass spectra were obtained from different ocular structures. This comparative study was best accomplished in the rat eyes, because we had access to all parts of the eye and optic nerve for analysis.

2.5.1 Optic nerve studies in *ex vivo* porcine eyes

Tissue to be subjected to imaging MALDI analysis was subjected to flash freezing by submersion in liquid nitrogen. Following the shock tube experiment, a section of the optic nerve was obtained from the eye, placed in a plastic, screw-cap, cryo storage vial, and plunged into liquid nitrogen. Samples from control eyes not exposed to blasts were similarly collected and frozen. After transport back to the laboratory, the samples were stored at -75° C until analysis.

To prepare tissue for MALDI analysis, sections were cut from frozen tissue specimens using a cryostat. Tissue sections were prepared following, in part, the protocol described by Grey et al. (2009). The frozen tissue block was mounted with TFM (a cryo mounting medium) on the cutting plate. With the cryostat temperature set to -24 to -27° C, 20- μ m thick frozen sections were cut from the optic nerve with the blade at a 6° cutting angle. The sections were transferred to indium titanium oxide (ITO)-coated slides, by touching the ITO-coated side to the sections still attached to the tissue block on the metal mounting plate in the cryostat. The slides were placed in a -20° C freezer until the methanol evaporated and the sections adhered to the ITO slides. The slides could be stored at -75 deg C until analysis time was available on the Bruker MALDI at UTSA.

In order to enhance the visibility of structures in the tissue, the sections were stained with 0.15% methylene blue. The mounted sections were first washed with distilled water and then stained for 8 – 10 sec in the methylene blue solution. Slides were then rinsed in an alcohol series: 1 min in 95% ethanol, two separate 1-minute rinses in 100% ethanol, and a final 5-min treatment with 100% xylene for 5 min. The stained slides were placed on filter paper and air-dried for 5 min. Prior to starting the MALDI analysis, the sections were visually inspected using a light microscope to identify structures of interest.

The matrix used for MALDI consists of an organic compound that facilitates the transfer of laser energy into the tissue and the ejection of protein or peptide fragments from the tissue and into the mass detector. Selecting the optimal matrix compound is an empirical process, beyond the general considerations of using a hydrophilic matrix compound for hydrophilic samples, and hydrophobic compounds for hydrophobic compounds. Several compounds were screened in preparation for the ocular trauma study, and sinapinic acid (3,5-dimethoxy-4-hydroxycinnamic acid; $C_{11}H_{12}O_5$) was found to produce the most consistent peaks from optic nerve samples. After application of the matrix compound, the tissue sections were dried under vacuum for at least 2 min and then placed in the Bruker MALDI instrument. The initial laser power setting was 28%, and then adjusted as necessary to obtain protein spectral peaks. The molecular mass range for the analysis was 7,000 to 50,000 amu. Sample spectra obtained from single locations in the optic nerve from porcine eyes are shown in Figures 17 and 18.

It may be appreciated that the spectra from the control eye (Figure 17) and eye subjected to a 4 disc blast (Figure 18) are similar, but not identical. There is a major peak at $m/z = 37,500$ in the control eye that is not present in the blast-subjected eye, and there is a sharp peak at $m/z = 12,200$ present in the blast eye that is absent in the control eye. It is doubtful that these differences represent novel proteins, because *ex vivo* tissue would not be expected to have the capability to express new proteins. These different protein patterns, however, may represent effects of sampling different ocular specimens, or perhaps differences in the metabolic state or stress level of the

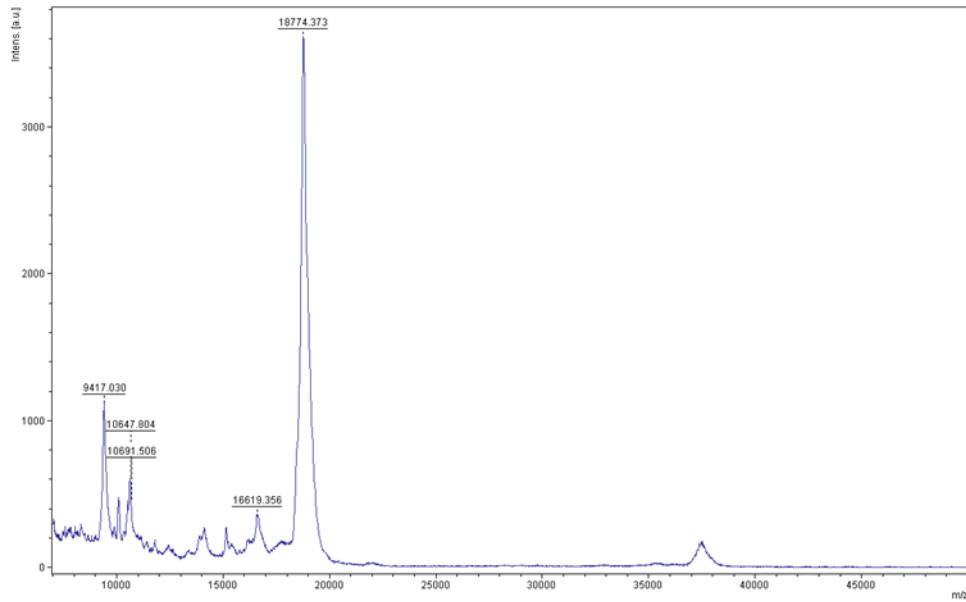


Figure 17. Mass spectrum of proteins ejected from optic nerve of a control (not exposed to a blast) porcine eye. Data obtained from a single location. Mass scan range was 7,000 to 50,000.

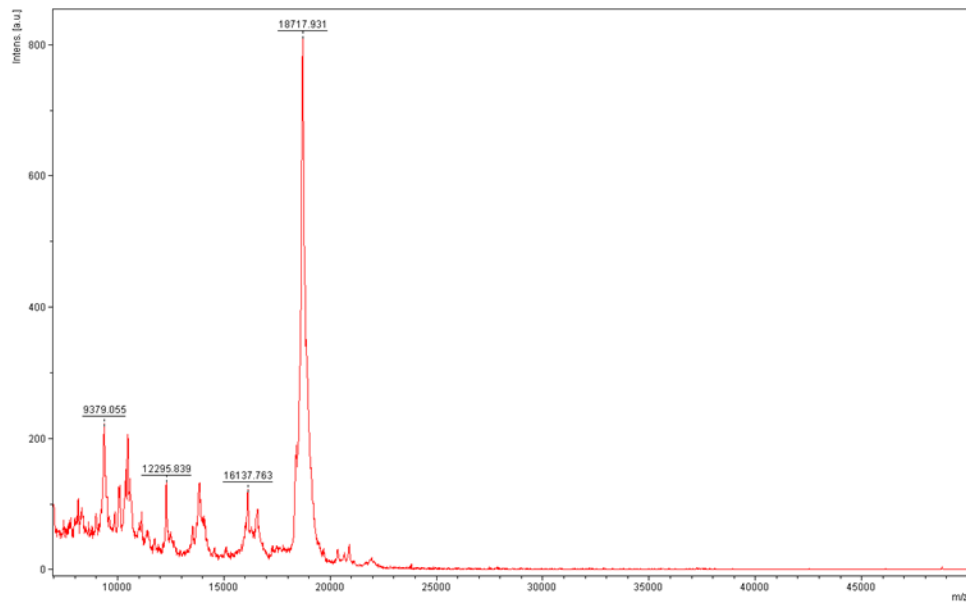


Figure 18. Mass spectrum of proteins ejected from the optic nerve of a porcine eye subjected to a 4 disc blast. MALDI parameters the same as for the control eye.

animals when they were slaughtered. We are not yet able to identify these proteins, because the UTSA group does not yet have the informatics portion of the MALDI system fully functional. Once this functionality is complete, we will be able to identify the sequence of the protein or peptide fragments detected based on their molecular weight, which will allow identification of the parent proteins.

Although the data shown here represent analyses taken at a single tissue location, “image” data may be constructed from individual measurements of this type, by stepping the activating laser across the tissue in a raster pattern and recording the intensity of the ejected ions (specifically, the mass/charge or m/z ratio) as a function of the position of the laser beam on the tissue. The resulting map of ion intensity vs. location produces an “image”, thus mapping the location of the protein being analyzed. It is expected that this approach will enable the detection and identification of novel protein biomarkers associated with optic nerve trauma.

2.5.2 Retina and optic nerve investigations in cadaver rats

In order to compare proteins expressed in retina and optic nerve, eyes were obtained from cadaver rats made available from an unrelated study. The eyes were dissected at various time points following the animal’s sacrifice, frozen and stored at -75°C as described above. The entire eye was mounted in the cryostat using TFM, and whole eye sections were cut and mounted on ITO-coated slides following the same protocol as for the porcine optic nerve samples. These sections were especially useful for comparing protein profiles from different sections; in the examples shown in Figures 19 and 10, the protein spectra were obtained from optic nerve (Figure 19) and lamina cribosa (the region where the optic nerve joins the retina, Figure 20). While there are several major protein moieties that are present in both locations, e.g. the peaks at $m/z = 12,000$ and at $14,100$ (note that there is a scale difference between these two figures), there are also many differences in the mass and abundance of proteins between these tissues, especially the protein grouping in the m/z range of $21,000$ to $24,000$ in the lamina cribosa that is completely absent in the optic nerve. Once the informatics functionality is available, these peaks will be identified, which will greatly aid in the search for trauma-specific biomarkers.

2.6 Trauma Data Analysis and Modeling

Although the development of predictive ocular trauma models will constitute the majority of our work in Year 3 of the project, preliminary work was undertaken this year in the development of trauma risk functions. Trauma risk functions estimate the probability of injury occurrence given some value of predictor variable, in this case peak blast pressure. To determine injury probability a logistic regression was performed for individual injury categories using the experimental and pathology data shown in Appendix II. A binary data set was generated whereby a positive pathology observation is taken to indicate a probability of 1 for the specific injury or injury category, and a

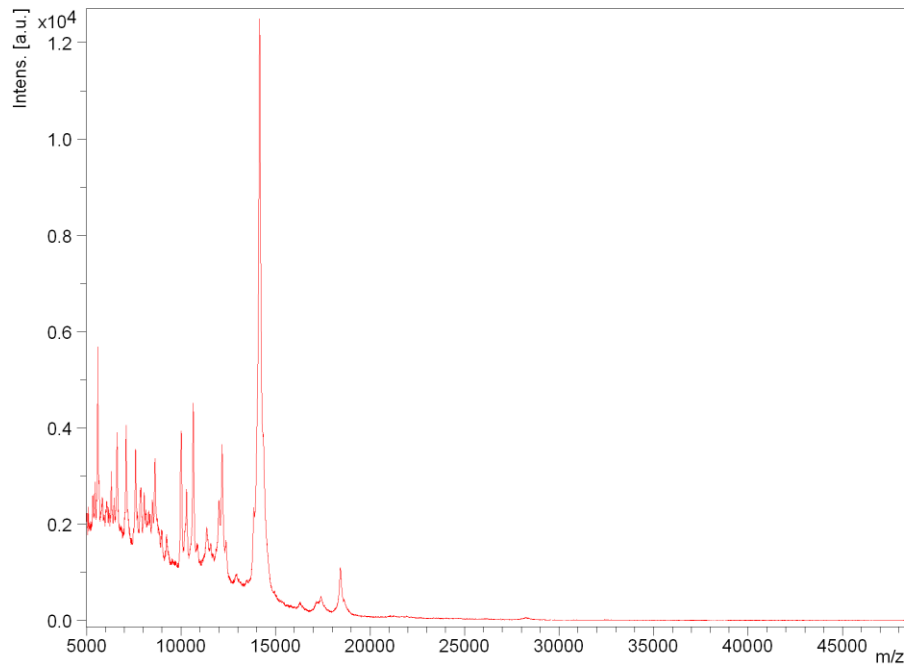


Figure 19. Mass spectrum of proteins ejected from rat optic nerve.

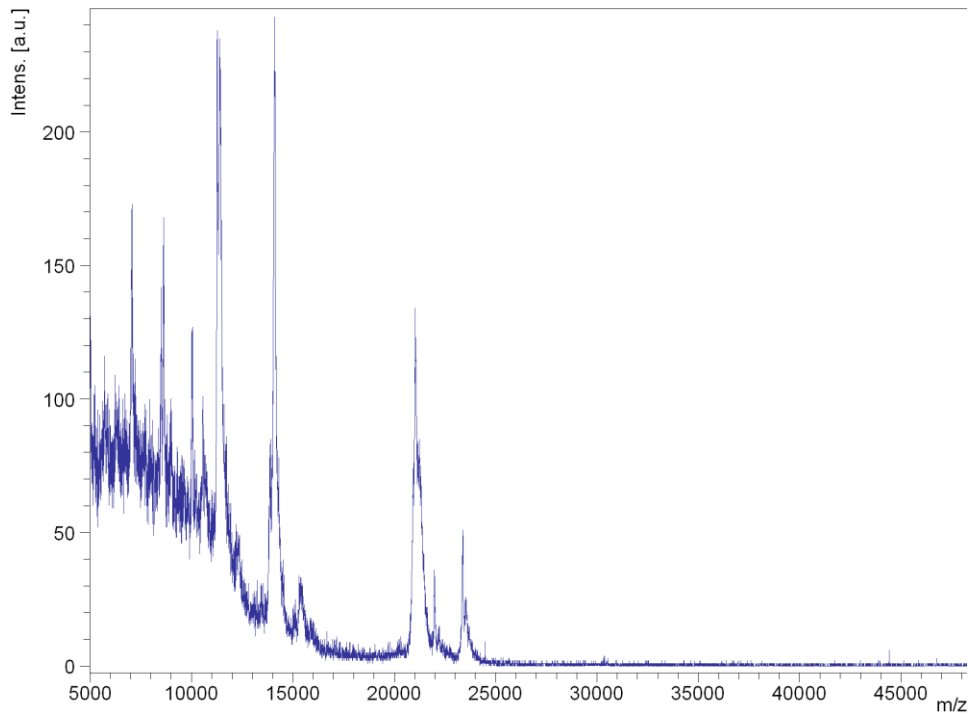


Figure 20. Mass spectra of proteins ejected from rat retina and optic nerve in the region of the lamina cribosa.

negative pathology observation is taken to indicate a probability of 0 (Collett, 2003). A logistic transformation and regression was then performed and the resulting coefficients input to the general form of the logistic risk function (Proud et al., 2009):

$$p = \frac{1}{1 + e^{-(ax+b)}}$$

where p is the probability of occurrence of the particular injury or trauma category. Following this method, probabilities of occurrence were calculated for each of the 12 injury categories (Figure 21). Individual response was plotted versus peak pressure and observations (positive observations in x-direction at a probability of 1, and negative observations in x-direction at probability of 0) are indicated by open circles. Probability of injury data could also be plotted versus blast impulse and energy. In future efforts we will explore these variations and determine which provide the best fit to data. It should be noted that corneal abrasion and retinal detachment were observed in the vast majority of post-test specimens and a significant number of control specimens, suggesting that these may be artifacts of the handling or pathology procedures. Although included in our preliminary development, future efforts will be aimed at determining the validity of these types of injuries in the blast environment.

Development of trauma risk functions has been hampered by the generally low tissue damage levels observed in the shock tube experiments. The maximum peak pressure achievable in the shock tube's current configuration is approximately 207 kPa (30 psi) and ~2 ms pulse width. At this shock condition, ocular tissue damage has been lower than expected. This may be due to the use of porcine, rather than human, eyes as porcine eyes are known to have a higher mechanical toughness than their human counterparts. As a result only a limited number of positive tissue damage observations are present in the binomial distributions, resulting in less than optimal conditions for plotting the probability curves (best fits result from approximately equal numbers of positive and negative observations). For example, some plots show that the chance of receiving injury is the same irrespective of increased incident pressure, the chance of receiving other injuries does not change with increased incident pressure, and—paradoxically—the chance of receiving some injuries is *lessened* with increased incident pressure. These seemingly nonsensical results may be caused by the scarcity of positive observations of tissue damage. In preliminary data reduction efforts we have shown that by the additional of just a few artificial positive observations (a few repeats at conditions that have already shown damage), the curves are greatly improved. Thus, it is hoped that additional tests with pulse widths approaching 4 ms will significantly increase the energy content of the blast wave, and in turn, increase the number of positive observations.

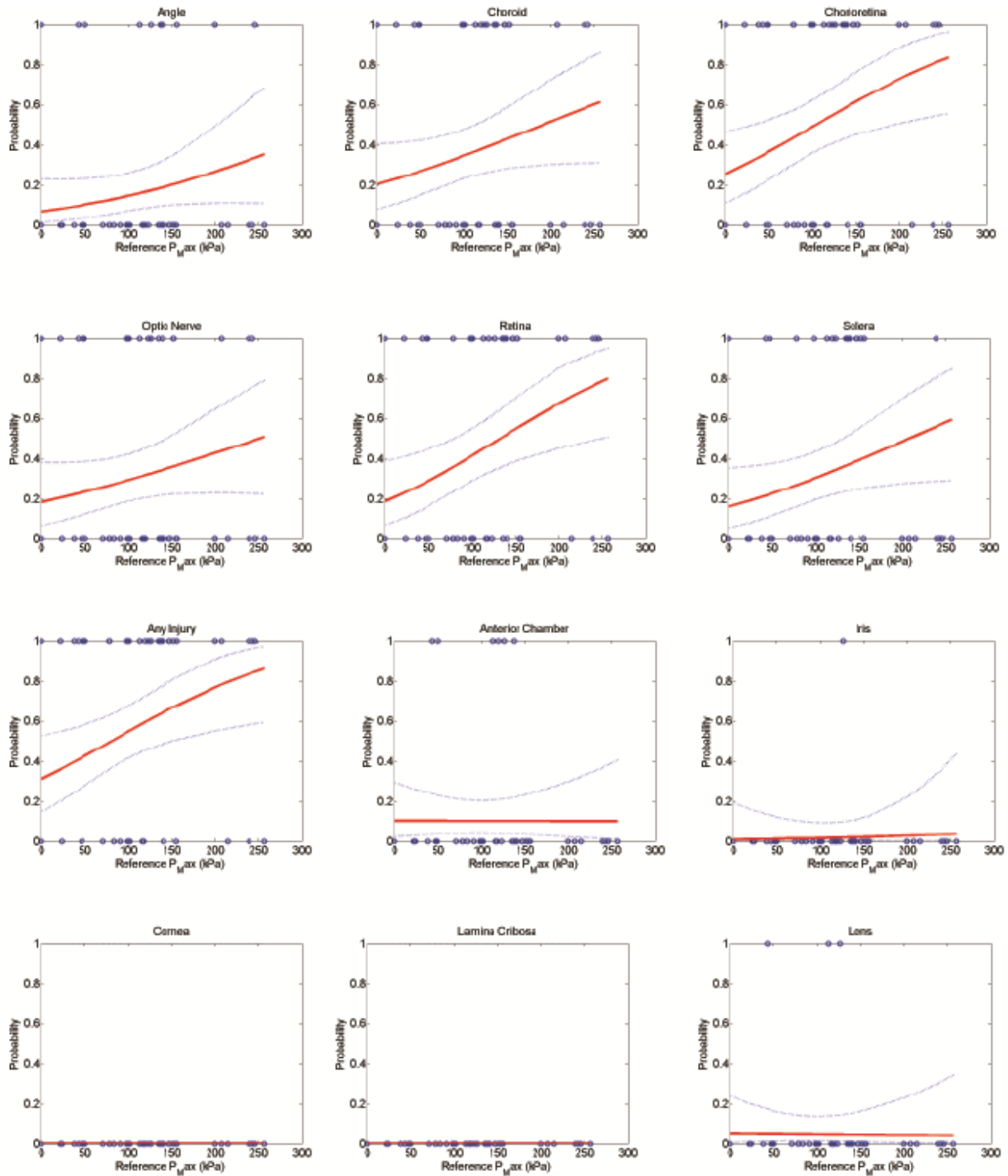


Figure 21. Preliminary ocular trauma risk functions vs. peak blast pressure. Trauma risk functions estimate the probability of injury occurrence given some value of predictor variable, in this case peak blast pressure. Corneal abrasion and retinal detachment were observed in the vast majority of post-test specimens and a significant number of control specimens, suggesting that these may be artifacts of the handling or pathology procedures.

2.7 Numerical Models & Simulations

Two computational software packages have been utilized to date to simulate the response of eyes to blast, LS-DYNA and CTH. An additional software package, EPIC, was recently received from US Army TARDEC, but has not yet been implemented. CTH is a three-dimensional Eulerian wave propagation code (hydrocode) developed and distributed by Sandia National Laboratories. It has a second order material advection algorithm and an advanced high-resolution interface tracker making it ideally suited for problems involving large distortions caused by blast or impact. In the Eulerian formulation the computational grid is fixed and materials are allowed to flow through the grid. After each time step, the materials and interfaces are re-projected back into the Eulerian grid avoiding many severe distortion problems commonly encountered in finite element codes such as LS-DYNA and EPIC.

LS-DYNA is a commercially available Lagrangian finite element program distributed by Livermore Software Technology Corporation (LSTC) of Livermore, California. It is generally considered the industry standard for simulation of vehicle crash and associated biomechanics. In the Lagrangian formulation, the computational grid remains fixed to the materials as they undergo distortion. Thus, large distortions often result in instabilities and early termination of the calculation. In LS-DYNA, the problem is partially solved by incorporation of Eulerian fluid dynamics components. We are using CTH to study the short-term effects of wave and shock propagation through the eye, and LS-DYNA (or EPIC) to study the longer term effects of acceleration and applied forces on the ocular tissues.

Due to delays in the obtaining ITAR approvals and delivery of the CTH and EPIC software packages, our initial efforts concentrated on development of an appropriate eye geometry model for input into LS-DYNA. Initial simulations with the model involved a spherical projectile impact event to allow comparison with previous work (Figure 22.) and as a check on the computational robustness of the model. Next, blast wave exposure of the eye was simulated using an empirical explosive-standoff model imbedded in LS-DYNA (CON WEP). This model generated the correct peak pressure when compared to the shock tube Friedlander wave, but the pulse width was much too long (Figure 23). Simulations using the CON WEP model at 48 kPa (7 psig) and 152 kPa (22 psig) peak pressures showed peak displacement occurred at the apex of the cornea; 1.54 mm of rearward displacement occurred at 1.11 milliseconds for the 48 kPa model, and 3.43 mm of displacement at 0.61 milliseconds for the 152 KPa model (Figure 24). Latest revisions to the LS-DYNA model have now allowed us to directly input measured pressure-time traces from actual shock tube blast experiments (Figure 3). Using the actual blast loading conditions should allow for direct comparison of simulations with experimental results, and thus provide a means for future validation of the model.

Two types of CTH computations have been undertaken to date, (1) simulations of the shock tube, and (2) simulations of the shock tube and eye. One disadvantage of CTH is that the blast wave must be generated within CTH from an initial static pressure

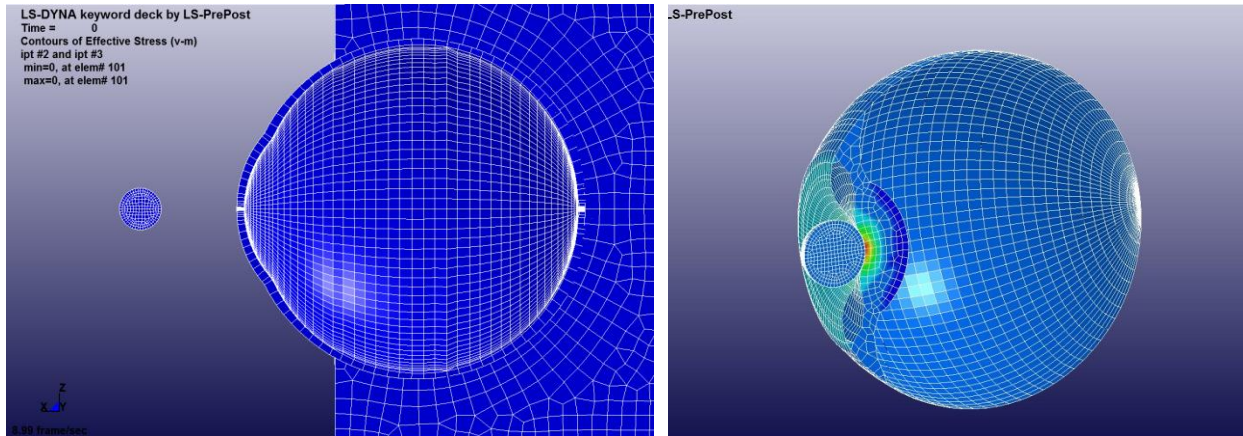


Figure 22. LS-DYNA numerical simulation of eye deformation due to spherical projectile impact. The projectile impact scenario was chosen to test the robustness of the geometric model. Impact is a more severe test of the model than blast.

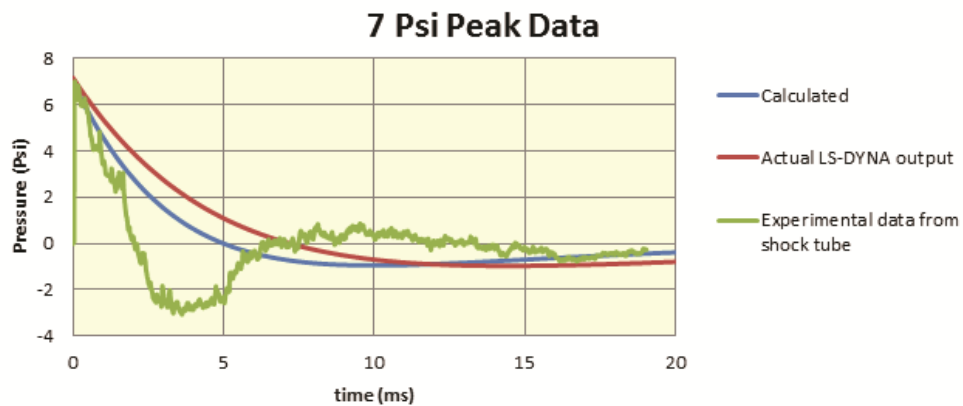


Figure 23. LS-DYNA calculated blast wave pressure-time histories (using CON WEP empirical model) compared to an actual Friedlander wave measured in shock tube experiments.

state. Thus to achieve the correct blast wave exposure, the entire shock tube must be modeled. As describe above, in LS-DYNA the blast wave can be input as an initial loading condition. In addition, CTH uses only solid elements requiring at least 4 elements across the 1 mm thick sclera. Thus, high fidelity CTH modeling of the shock tube and eye requires models with in excess of 1 million computational elements, and very long run times (currently on the order of 1 week of actual time). LS-DYNA on the other hand can utilize single membrane elements (of defined thickness) for some of the interior structures of the eye.

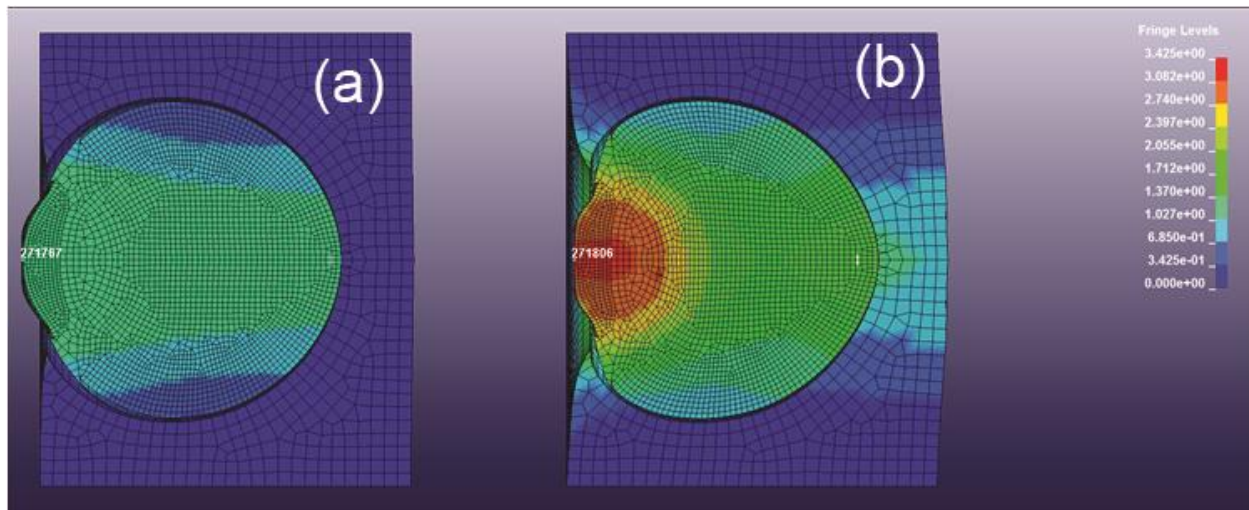


Figure 24. Eye displacements calculated in LS-DYNA using the CON WEP empirical pressure model for (a) 48 kPa and (b) 152 kPa peak pressure.

2.7.1 LS-DYNA

Geometry for a Finite Element Analysis (FEA) model of the human eye was created in 3D using the SolidWorks CAD software. Dimensional data for the model came from a variety of sources (Table 2). This model was created alongside the physical experiments conducted with a shock tube. In these experiments the eye was held in an acrylic holder filled with gelatin that mimicked the bony orbit and muscle tissue surrounding the eye. The eye/holder was then exposed to blast at various levels. The level of detail in the eye model was chosen as a compromise between computational efficiency and anatomical detail.

The 3D geometry was meshed and assembled using the LS-PrePost software for use with the LS-DYNA FEA software (Livermore Software Technology Corporation, Livermore, CA). LS-DYNA is a general purpose finite element code for analyzing large deformation dynamic response of structures. [LS DYNA MANUAL]. The explicit solver was used for this study. Figure 25 shows the FEA model and mesh. The model consisted of 10 parts; cornea, sclera, choroid, retina, vitreous, lens, zonules, ciliary body, aqueous, and surrounding gelatin. 8 node brick and 4 node tetrahedral solid elements were used throughout, with a total of 381,623 elements. All components of the eye were modeled with a Lagrangian mesh. The cornea, sclera, choroid, retina, ciliary body, zonules, and lens were attached at their respective interfaces. The aqueous and vitreous were bounded by contact with their chambers, but not attached. The eye model was bounded by contact, but not attached to the gelatin. The eye and gelatin were modeled in quarter symmetry with mirrored boundary conditions at the sectional

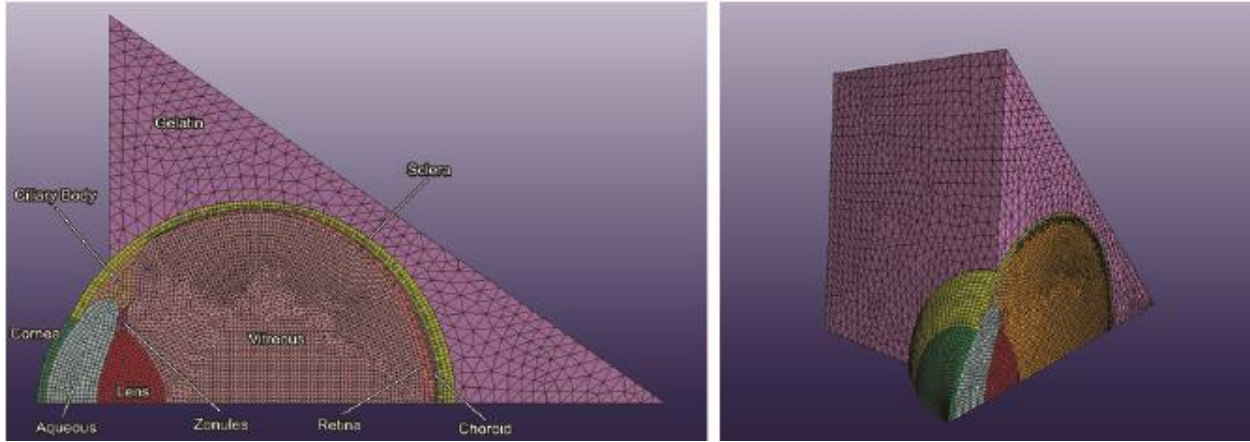


Figure 25. Cross section and isometric views of quarter symmetry model and mesh implemented in LS-DYNA. Dimensional and material properties used in the model are presented in Tables 1 and 2, respectively.

Table 2. Dimensional data for FEA model

Geometry	Dimensional Value	Source
Scleral outer radius	12 mm	Bron et al 1997
Scleral inner radii	various	Olsen 1998
Corneal outer radius	7.8 mm	Bron et al 1997
Corneal thickness	0.52 - 0.6 mm	Bron et al 1997
Lens anterior radius	fit to equation	Burd 2002
Lens posterior radius	fit to equation	Burd 2002
Lens position	3 mm posterior to posterior surface of cornea	Bron et al 1997
Zonules	Simplified for simulation purposes. Geometry based on refs.	Burd 2002, Bron et al 1997
Ciliary body	Simplified for simulation purposes. Geometry based on ch 6 figures and dimensions.	Bron et al 1997
Iris root thickness	0.5 mm	Bron et al 1997
Iris collarette thickness	0.6 mm	Bron et al 1997
Pupil diameter	3 mm	Bron et al 1997
Choroid thickness	0.1 - 0.3 mm	Bron et al 1997
Retina thickness	.01 - 0.56 mm	Bron et al 1997

interfaces. Rigid boundary conditions were applied to the gelatin at contact surfaces with the acrylic holder. The holder itself was not modeled.

Linear elastic material models were used for all parts except the aqueous and vitreous, which were modeled with a linear elastic fluid model. The model material properties are reported in Table 3. A broad range of material properties have been reported in the literature. Those chosen for the model were within the range of other FEA studies done on the eye. Loading conditions for the FEA model were taken from experimental data measured in the shock tube. Pressure history data were applied to the exposed anterior surfaces of the cornea, sclera, and gelatin. Three levels of blast corresponding to peak overpressures of 48 kPa, 96 kPa, and 151 kPa (8, 14, and 22

Table 3. Material properties used in FEA model

Part	Density (g/mm ³)	Youngs Modulus (Mpa)	Bulk Modulus (Mpa)	Poissons Ratio	Source of Material Properties
Aqueous	0.0010	-	2200	0.49	Fox 2004
Choroid	0.0010	0.05	-	0.47	Sigal 2004
Ciliary	0.0016	11	-	0.45	Power 2001
Cornea	0.0014	14	-	0.45	Uchio 1999
Gelatin	0.0010	0.5	-	0.49	Power 2001
Lens	0.0011	6.9	-	0.48	Stitzel 2002
Retina	0.0010	0.05	-	0.47	Sigal 2004
Sclera	0.0014	35	-	0.45	Uchio 1999
Vitreous	0.0010	-	2200	0.49	Fox 2004
Zonules	0.0010	35	-	0.45	Stitzel 2002

psi, respectively) were modeled. Only the positive phase of the pressure history was used, simulating 2 ms of real time. Simulations were run using 64 CPUs of a 192 CPU High Performance Computing (HPC) cluster. Run time for each simulation was approximately 9 days.

A softer material stiffness with the goal of obtaining fully run models at the 48, 96, and 151 KPa levels has recently been implemented. For these models the card “Force_Transducer_Penalty” was added, allowing for calculation of the force between the vitreous and retina, and between the retina and sclera. We have also experimented with non-linear material models for the cornea and sclera, specifically the *Mat_Mooney-Rivlin_Rubber model. The rationale for using this model is the softening with increasing strain of the Uchio et al. (1999) data for the cornea and sclera (Figure 26). When LS DYNA detects the initial deformation, the stress-strain curve is interpolated based on the given elastic modulus. With a simple elastic modulus definition, the interpolation happens along the given slope, but with softening it follows the non-linear curve like that given by Uchio et al. (1999). The idea is that interpolation will occur along a less steep slope, leading to a less severe initial perturbation. The LS DYNA Mooney-Rivlin model allows user input of a stress-strain curve.

Analysis of the completed runs reveals the dynamics of the models. Figure 27 shows a time sequence displaying one of the more interesting aspects. The leftmost frame shows the 150 kPa model at 440 microseconds. At this point the blast wave has imparted horizontal direction velocity to the model causing all components to move posteriorly. At 610 microseconds the sclera has slowed in its movement into the gelatin while the vitreous has continued rearward compressing the chorioretina between the vitreous and the sclera. At 1740 microseconds the vitreous has rebounded anteriorly, pulling away from the chorioretina. This sequence, in which the retina is first crushed then pulled by the vitreous, appears to have implications as a mechanism for retinal detachment due to primary blast.

Response of the model to the three blast profiles was characterized by displacements of the cornea and sclera, change in thickness of the retina, overall change in length of the globe, and force on the retina (Figure 28). Force was measured

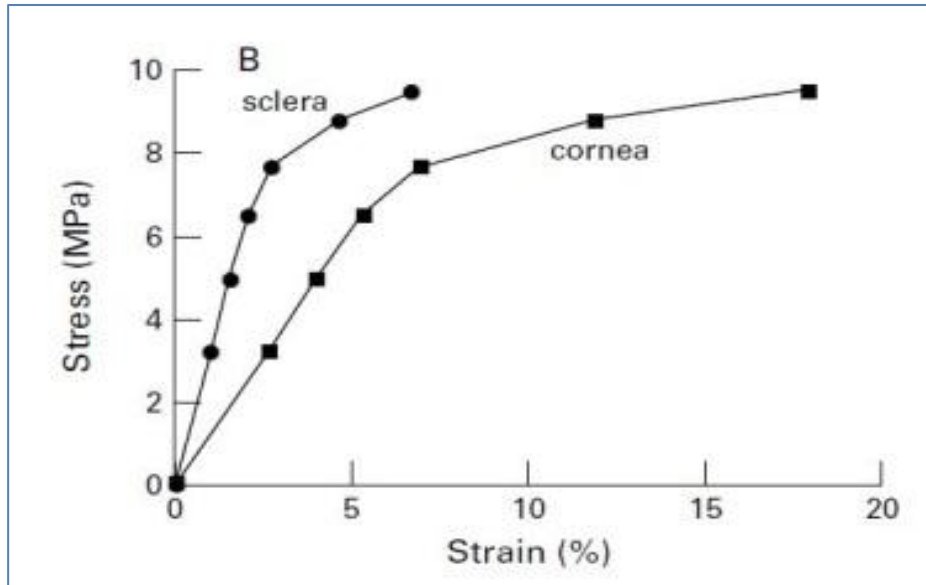


Figure 26. Stress strain for cornea and sclera from Uchio et al., 1999.

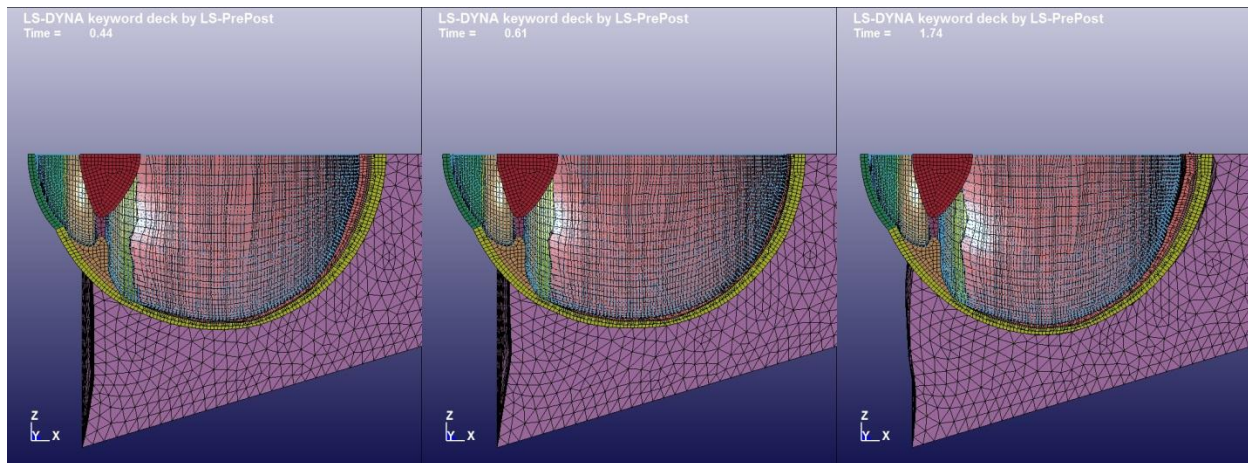


Figure 27. 151 kPa eye model at 440, 610, and 1740 microseconds, from left to right. In this sequence the retina is first crushed, then pulled away from the chorioretina. This phenomenon may have implications as to mechanism for retinal detachments during primary blast.

between the vitreous and retina. The posterior displacements in the cornea and scleral apex are not surprising given the compressive nature of the blast wave, but the change in retinal thickness is surprising. The simulations reveal an initial compression followed by tensile expansion as the blast wave propagates through the eye. This behavior is also shown in the force transmitted to the retina. This oscillatory behavior may explain the ubiquitous chorioretina detachments observed in the post-blast pathology.

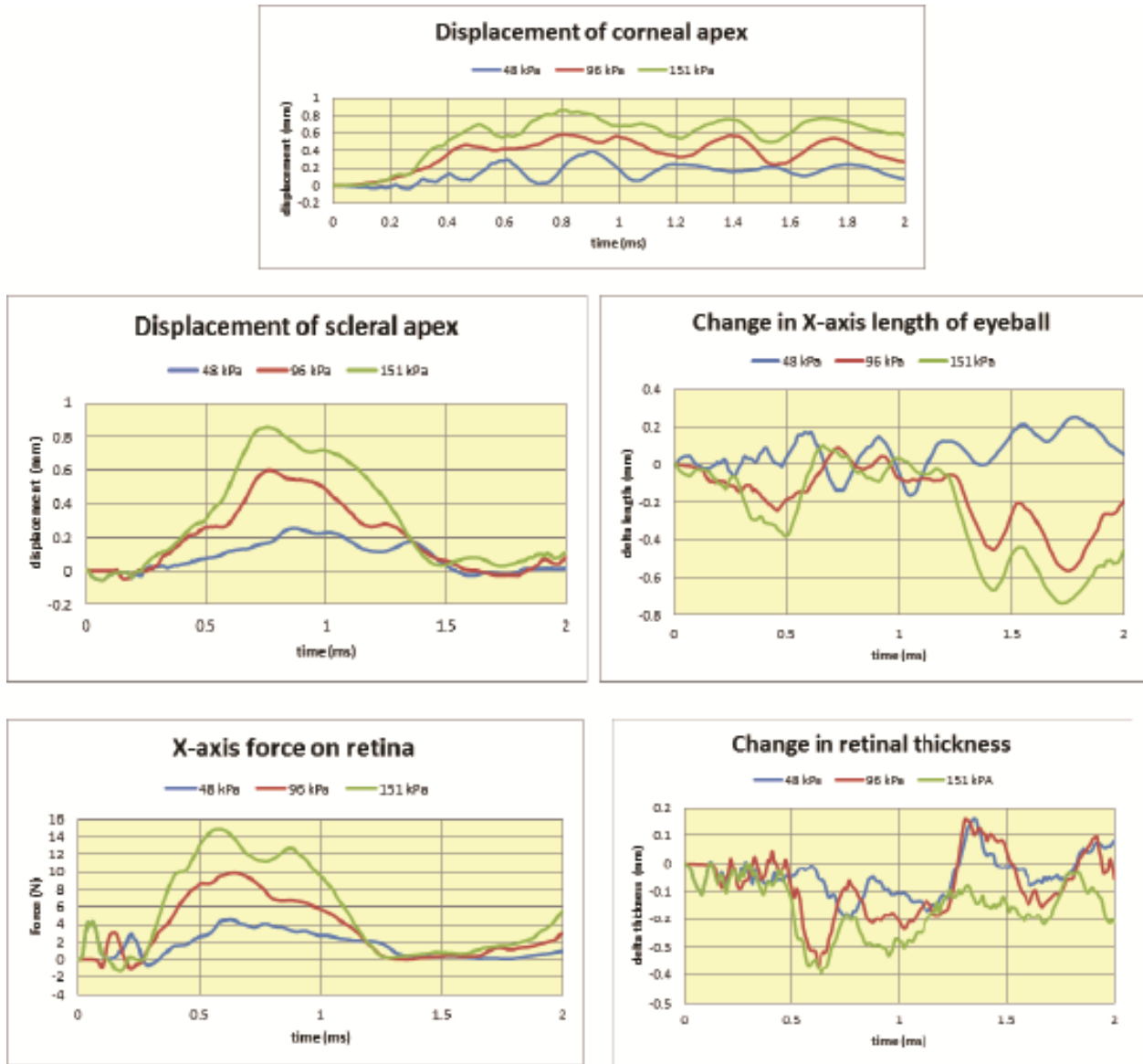


Figure 28. Response of the LS-DYNA eye model using the Uchio (Uchio et al., 1999) “softened” elastic modulus (Figure 21).

2.7.2 CTH

CTH was received at UTSA in February, with initial efforts focused on modeling blast wave generation in the shock tube. The objective was to investigate the initial loading conditions required to generate Friedlander waveforms similar to those observed in the porcine eye experiments, i.e., sharp shock front with correct peak

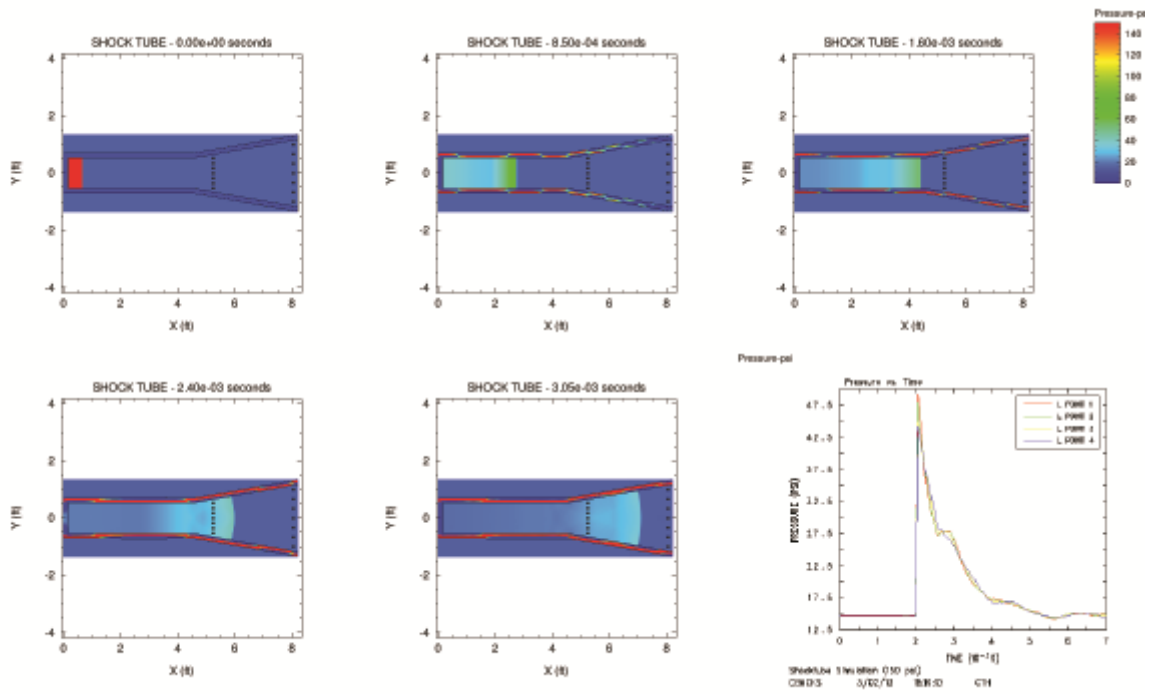


Figure 29. CTH simulation of the shock tube. The simulation is started by placing a volume of high pressure air at the upstream end and allowing it to propagate down the tube. The shock front (Friedlander waveform) develops at the open end.

pressure and pulse width. Unlike LS-DYNA where the pressure-time history can be directly input to the program, CTH must generate the waveform as part of the computation. In this case, a volume of high pressure air is placed in the upstream end of the shock tube and allowed to propagate toward the open end of the shock tube. This is analogous to pressurizing the shock tube’s driver section and allowing the aluminum disk to rupture. As air propagates down the tube, a shock front or Friedlander waveform develops (Figure 29).

Due to symmetry, a 2-D geometrical model was deemed adequate for simulating the performance of the shock tube. Each computational cell was 0.25 x 0.25 cm in size resulting in a total of 164,000 cells. An embedded tabular equation of state model (SESAME table) was used to simulate the air, and the shock tube is modeled as a rigid (impermeable, non-moveable) material. In the initial trials the correct pulse width (~ 2 ms) was consistently achieved for a number of peak pressures, but the negative pressure phase (see Figure 3) was not achieved. However, through trial and error we were able to replicate this by using a sound speed absorbing boundary condition (condition 1 in CTH) at the open end of the tube. The choice of this particular boundary condition was not an obvious choice, as our first inclination was to allow the air to exit the open end (condition 2 in CTH). However, this did not consistently produce the

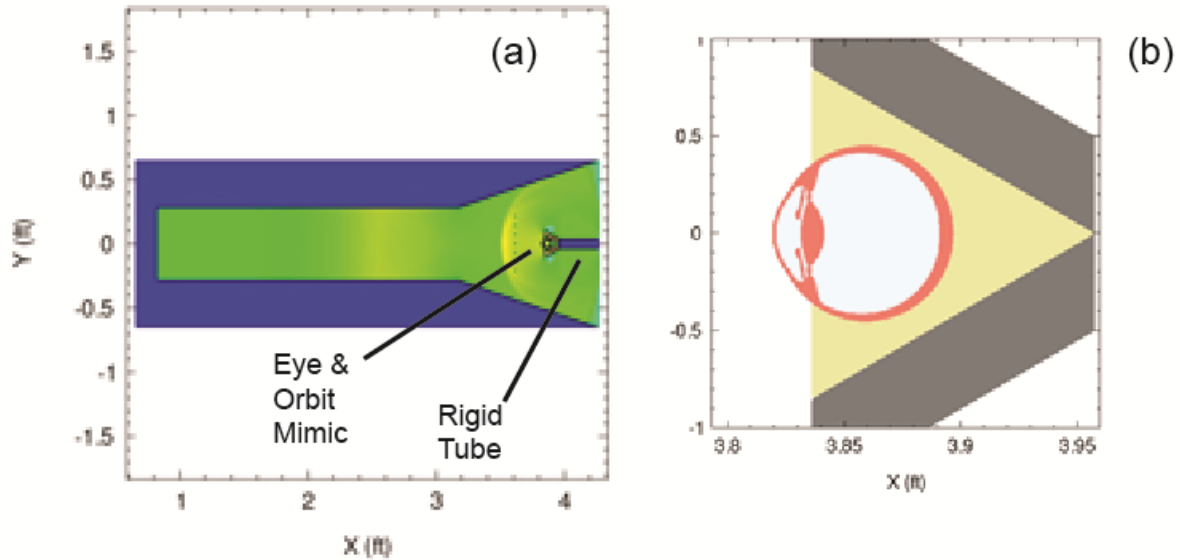


Figure 30. (a) CTH model of the shock tube with eye-orbit mimic included. The eye-orbit assembly is held in place by a rigid tube that is not allowed to move during the computations. (b) Close up of the eye-orbit mimic model. Note that gelatin is placed between the eye and orbit mimic to simulate the extraocular muscles.

desired negative pressure phase, and on occasion caused the computation to terminate early due to mass balance errors. CTH assumes mass conservation in the calculations, so letting mass exit the computational grid sometimes results in non-convergence during iteration.

The next series of CTH computations placed an eye-orbit mimic model at the open end of the tube in a configuration similar to that employed in the porcine eye experiments (Figure 30). The eye-orbit mimic assembly was held in place with a rigid tube that was fixed in place (not allowed to move in the computations) and extended out the open end of the tube. Due to the rotational symmetry of the eye, an axisymmetric model was utilized with the eye centerline as the axis of rotation. The small thickness of the ocular tissues (e.g., sclera ~ 1 mm) required a much more refined grid than was used in the shock tube simulations. A grid size of 0.20 x 0.20 cm was chosen to ensure at least 5 computational cells across the scleral thickness. This resulted in approximately 1.4 million computational cells with run times in excess of 1 week.

Dimensional and geometric details of the eye and orbit were taken predominately from a single reference; Wolff's Anatomy of the Eye and Orbit, 8th Edition (Bron et al., 2001). The structures important to modeling dynamic response and trauma were identified as the cornea, aqueous humor, iris, zonule, lens, vitreous, sclera, retina, and choroid (Figure 30b). The sclera, retina, and choroid have been combined into a single scleral shell as modeling the individual layers is not practical in CTH (due to their thinness). However, it has been shown in previous work that deformation and strain partitioning can be adequately modeled using a single scleral shell approach.

Representative mechanical properties of the ocular tissues used in the CTH model are presented in Table 4. The heat capacity, Gúneisen Parameter, and Up-Us slope (slope of Hugoniot curve) of all tissues were taken to be those of water. This assumption was considered reasonable as human tissue is thought to contain considerable water either in solution or suspension. In the simple model the retina, choroid, and sclera were modeled as a single membrane using the scleral properties. To simulate material response, a Mie-Grúneisen equation of state and a modified Johnson-Cooke constitutive model were used for each tissue.

A number of CTH calculations at the various blast pressure conditions observed in the porcine experiments are currently underway. Consistent with experimental observations, peak blast pressures in the 48 kPa to 151 kPa range are producing low levels of stress and strain in the eyes, mostly in the corneal and scleral region (Figure 31). In early times (associated with blast wave arrival) stress is concentrated in the cornea, but propagates to the mid- and posterior scleral regions in late times. The propagating stress may be due to a minor flattening of the globe from pressure loading or simply a response to interior pressure wave propagation. In most of the simulations pressure reflections off the posterior can be observed (Figure 32). Our previous research with blunt impact events suggests that such reflections may be responsible for retinal detachments.

Table 4. Mechanical Properties of the Ocular Tissues

	Density kg/m ³	Young's Modulus (Pa)	Poisson's Ratio	Sound Speed (m/s)	Yield Stress (Pa)	Failure Stress (Pa)	Heat Capacity J/(kg-K)	Guneisen Parameter	Up-Us Slope
Optic nerve	1400	6.56E+06	0.49	1540	1.50E+03		3664	0.1	2
Retina	1400	5.20E+03					3664	0.1	2
Dura	1400	3.58E+08	0.47	1540	9.40E+06	9.49E+06	3664	0.1	2
Lens	1079	6.89E+06	0.49	1540		1.75E+07	3664	0.1	2
Cornea	1400	1.24E+08	0.42	1540	9.40E+06	9.45E+06	3664	0.1	2
Iris	1400	1.24E+08	0.42	1540	9.40E+06	9.45E+06	3664	0.1	2
Ciliary Body	1400	3.58E+08	0.47	1540	9.40E+06	9.49E+06	3664	0.1	2
Zonule	1000	3.58E+08		1540			3664	0.1	2
Sclera	1400	3.58E+08	0.47	1540	9.40E+06	9.49E+06	3664	0.1	2
Choroid	1400	3.58E+08	0.47	1540	9.40E+06	9.49E+06	3664	0.1	2
Aqueous Humor	1003	--	--	1503	--	--	3664	0.1	2
Vitreous	1009	1.54E+05	0.49	1528	1.0E+1	1.57E+05	3664	0.1	2
Orbital Bone	1610	9.81E+10	0.35	2503	1.57E+08	1.57E+08	1256	0.1	2

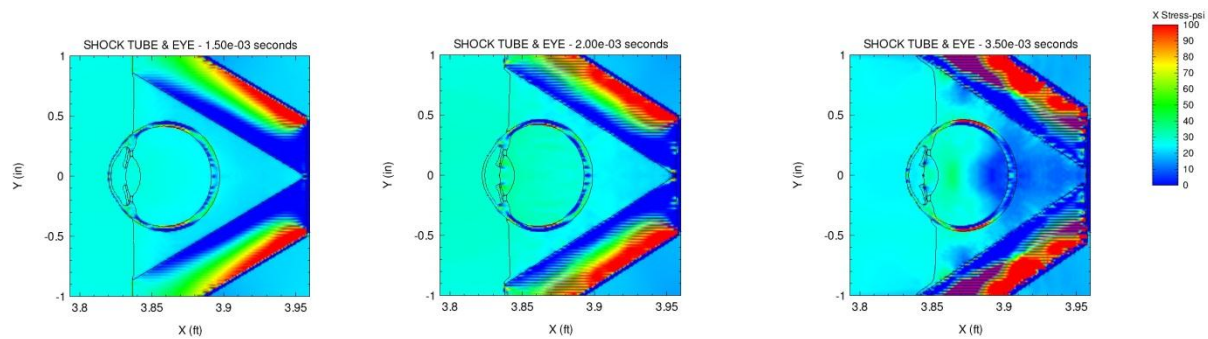


Figure 31. CTH simulation of 151 kPa peak pressure showing development of low level stress (~100 psi) in the mid-sclera regions of the eye. CTH simulations have shown that in early times stress is concentrated in the cornea, but propagates to the scleral regions at late times

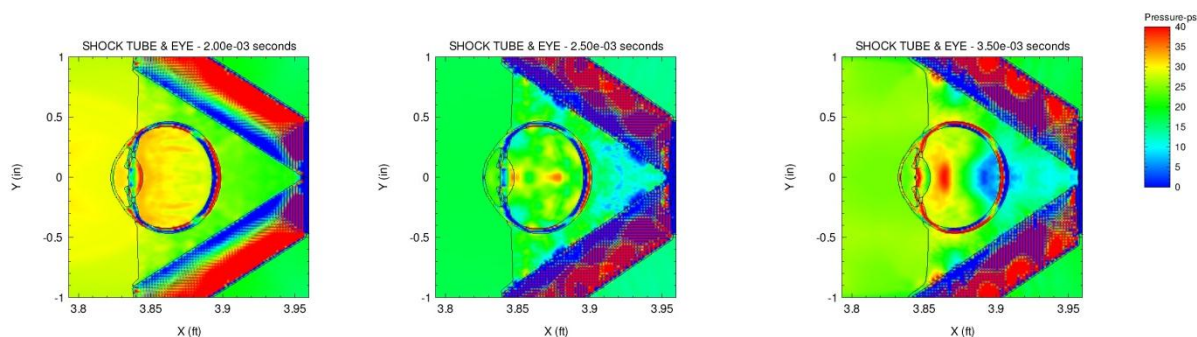


Figure 32. CTH simulation at 151 kPa peak pressure showing pressure reflection off posterior. Previous research has suggested that such reflections may be responsible for retinal detachments.

3.0 KEY RESEARCH ACCOMPLISHMENTS

- Completion of 68 shock tube experiments on porcine eye specimens. Detailed procedures for preparation and blast testing of eye specimens have been developed and validated. These procedures will guide development of protocols for *in vivo* rabbit testing during year 2 of the project.
- Completion of preliminary pathology (including assessment of trauma types and levels) on 96 porcine eye specimens (68 blast exposures and 28 controls). To date the pathology assessment has relied on post-blast screening using ultrasound techniques (UBM and B-scan), supplemented by limited dissection and histopathology. In the future we hope to increase the number of eye specimens subjected to detailed histopathology. The ultrasound techniques

provide clear information about the chorioretina (pre- and post-impact), but are unable to adequately resolve trauma in the angle region. Although dissection and histopathology can resolve trauma in the angle region, the potential for artifact is increased. It is hoped that future application of both techniques will be successful in providing a more complete picture of the trauma.

- Development of rigorous control procedures that allow an estimation of the relative effects of shipping, handling, mounting, preparation, tissue degradation, and repressurization of the globe in development of injuries not related to primary blast. These controls are included in every blast test performed.
- Development of a scoring methodology on a per-tissue basis that allows for interpretation in the framework of the OTCS zone-based scoring system.
- Preliminary development of trauma risk curves for a number of sub-globe-rupture trauma categories. However, the effort has been hampered by the generally low tissue damage levels observed in the shock tube experiments. We are evaluating options for increasing the overall impulse and energy delivered by the ISR shock tube, as well as other techniques for evaluation of the data and model building.
- Completion of preliminary numerical simulations using software packages CTH and LS-DYNA. The LS-DYNA simulations have been particularly fruitful in revealing mechanical response that contributes to chorioretinal trauma, namely oscillatory compression and tension on the retina during wave propagation through the eye. Separation of the vitreous and retina, as observed in the simulations, may contribute to retinal detachments.
- Optic nerve specimens have been successfully cut and mounted in preparation for imaging using the Matrix Assisted Laser Desorption Ionization (MALDI) technique. The sections were mounted on the ITO slides from a methanol layer, and appear to have attached well on to the slides after evaporation of the methanol. Trauma-related proteins will be identified by the homology of the measured m/z spectra with protein sequences published in the UniProt database

4.0 REPORTABLE OUTCOMES

Two abstracts/posters submitted by the team were presented at the 2013 ARVO Meeting in Seattle:

(1) A Computational Models for Investigation of Ocular Trauma Due to Primary Blast

Presentation Number: 3045
Posterboard Number: C0208
Session Number: 321
Session Title: Anatomy

(2) Primary Blast-Induced Ocular Trauma Modulated by Peak Pressure

Presentation Number: 3043
Posterboard Number: C0206
Session Number: 321
Session Title: Anatomy

One abstract/poster submitted by the team was presented at the 2013 ASME Summer Bioengineering Conference in Sunriver:

- (1) Manifestation of primary Blast-Induced Ocular Trauma
Presentation Number: SBC2013-14446
Session Title: Ocular Biomechanics

One abstract/poster submitted by the team has been accepted for the Biomedical Engineering Society (BMES) Annual Meeting, September 25-28, 2013 in Seattle:

- (1) Primary Blast-Induced Ocular Trauma
Submission ID: 2573
Submission Title: Submission Track: Biomechanics
Submission Subtrack: Other/Non-Specified

5.0 CONCLUSIONS

The data generated in in this study has significantly increased our understanding of primary blast-induced ocular injury. This shock tube produced a broad array of closed-globe injuries, many of which would seriously compromise visual function. The experimental techniques and injury characterization methodologies offer an objective assessment as to which injuries were due to blast exposure. Pre-imaging each eye using ultrasound allowed exclusion of eyes that would otherwise contribute artifacts and improves confidence that any damage to the eye after blast exposure is due only to the effects of primary blast rather than preparation or other factor.

A notable strength of this study is the evaluation of the blast trauma with the complimentary methods including UBM, B-scan, gross dissection and histopathology. Specifically, our results show that ultrasound scans give clear information about the chorioretina (pre- and post-impact) while dissection can result in artifact. Conversely, the ultrasound methods were unable to resolve angle recession while histological sections gave more reliable information regarding anterior segment damage. In combination these modalities assist in the primary objective of identifying intraocular injuries that could have lifelong adverse effects.

Previous blunt impact studies conducted with paintballs found an ocular damage threshold of 2-13.5 J (Sponsel et al., 2011). The present study found a similar increasing trend in ocular damage with increasing blast energies, but globe distortion and movement were far less than in the paintball study. This may be due to several factors such as the lower energies associated with the blast, simultaneous compression of the periorbita, and distribution of the energy over the entire exposed surface rather than concentrating the load at the point of projectile impact. None the less, we observed a broad array of ocular injuries. Petras et al. (1997) observed a similar trend in rats exposed to overpressures of 104 –173 kPa (15-25 psi).

For this study we chose to use porcine eyes to eliminate effects due to age, health history, and other uncontrollable factors. However, porcine eyes are known to have a higher mechanical strength than human eyes (Kennedy et al., 2007), suggesting that blast conditions that produce injuries in porcine eyes will likely induce more serious injuries in the human eye. Thus, the injury data generated from porcine eyes should give conservative estimates of injuries which might occur in human eyes during primary blast events.

Control eyes experienced some apparent damage which was clearly not due to blast exposure. This may indicate continual degradation of the porcine eyes after the pre-screening ultrasound was performed, damage inflicted to the eye due to the presence of the gelatin and/or hot lights required for high-speed video, or other artifacts of the preparation. Still, incidence and severity of damage in the exposed eyes was significantly correlated with the impulse indicating that primary blast modulated these injuries.

Ocular trauma scores describe a range of open and closed globe injuries. Current ocular trauma scores, like the Ocular Trauma Classification System (OTCS) or the Birmingham Eye Trauma Terminology (BETT; Kuhn et al., 2004) subdivide open globe injuries between lacerations and ruptures while subdividing closed globe injuries between contusions and lamellar lacerations. Cockerham et al. (2009) noted a need for the development of a universal parlance in describing blast-related ocular injuries. Such a scale must account for the full range of ocular injuries from the subtle, closed-globe nature of primary blast injuries observed here through globe rupture.

Continued experimentation in this area will allow more robust correlation between the blast wave characteristics and frequency of trauma response. Ultimately, a probabilistic regression model predicting the likelihood of a specific type of injury similar to the Bowen curves will enable informed treatment by medical staff. Our parallel computational studies seek to use numerical modeling of blast exposure to understand the mechanisms of these injuries, similar to the approach recently undertaken by Bhardwaj et al. (2013). The modeling should soon provide rapid, inexpensive methods for testing various protective eyewear solutions which might mitigate blast damage to the eye.

The computational eye models provided the opportunity to visualize the interior structures of a surrogate eye during the extreme dynamics of a blast event and provided insight into mechanisms of primary blast injury. Of particular interest was the response of the LS-DYNA model at the interface of the vitreous and retina. A series of snapshots of the model progressing forward in time shows contours the motion of the vitreous as it encounters the retina, compressing it and the choroid against the sclera (Figures 22 & 23). This compression is followed by rebound of the vitreous away from the retina. Given the reported tensile strength of the choroid and retina, this finding indicates a high likelihood of damage to the retina via the interaction with the vitreous in both tension and compression. The degree of compression of the retina was related to the peak overpressure, with maximum compression occurring in both the 96 kPa and 151 kPa simulations. The 48 kPa simulation showed very little compression of the retina. Statistical analysis of the physical experiments also showed increasing risk of retinal injury with the higher peak overpressures.

REFERENCES

- Bhardwaj, R., Ziegler, K., Seo, J.H., Ramesh, K.T., and Nguyen, T.D., 2013, A computational model of blast loading of the human eye: *Biomech Model Mechanobiol*, v. 17 (Epub ahead of print, April 2013).
- Bowen, I.G., Fletcher, E.R., and Richmond, D.R., 1968, Estimate of Man's tolerance to direct effects of air blast: Defense Atomic Support Agency Report, DASA 2113, 44 p.
- Cockerham, G.C., Goodrich, G.L., Weichel, E.D., 2009, Eye and visual function in traumatic brain injury: *J Rehab Res Dev.*, v. 46, pp. 811-818.
- Collett, D., 2003, *Modeling Binary Data*: Chapman & Hall, 228 p.
- Duma, S.M., Ng, T.P., Kennedy, E.A., Stitzel, J.D., Hering, I.P., and Kuhn, F., 2005, Determination of significant parameters for eye injury risk from projectiles: *Journal of Trauma*, v.59, pp. 960-964.
- Duma S, and Kennedy, E., 2011, Final Report: Eye Injury Risk Functions for Human and FOCUS Eyes: Hyphema, Lens Dislocation and Retinal Damage: USAMRMC report W*!XWH-05-2-0055, 66 p.
- Gray, W., Weiss, C.E., Bonivitch, A.R., Sponsel, W.E., Scribbick, F. W., Miller, P., Armstrong, A.A., Walker, J.D., and Nicolella, D.P., 2008a, Modeling of paintball ocular trauma: A path towards development of an impact and blunt trauma predictive capability: SwRI Internal Research Report No. 18.R9664, 59 p.

- Gray, W., Weiss, C.E., Sponsel, W. E, 2008b, Computational and experimental study of paintball impact ocular trauma: Proceedings 24th International Symposium on Ballistics, pp 1260-1267.
- Gray, W., Sponsel, W.E., Scribbick, F.W., Stern, A.R., Weiss, C.E., Groth, S.L., and Walker, J.D., 2011, Numerical modeling of paintball impact ocular trauma: Identification of progressive injury mechanisms: Investigative Ophthalmology and Visual Science, v. 52, pp. 7506-7513.
- Grey, A.C., Chaurand, P., Caprioli, R.M., Schey, K.L., 2009, MALDI imaging mass spectrometry of integral membrane proteins from ocular lens and retinal tissue: J. Proteome Res. V. 8, pp. 3278-3283.
- Kennedy, E.A., Voorhies, K.D., Herring, J.P., Rath, A.L., and Duma, S.M., 2004, Prediction of severe eye injuries in automobile accidents static and dynamic rupture of the eye: Annu Proc Assoc Adv Automot Med, v. 48, pp. 165-179.
- Kennedy, E.A., Ng, T.P., McNally, C., Stitzel, J.D., and Duma, S.M., 2006, Risk functions for human and porcine eye rupture based on projectile characteristics of blunt objects: Stapp Car Crash Journal, v. 50, pp. 651-671.
- Kennedy, E.A., McNally, C., and Duma, S.M., 2007, Experimental techniques for measuring the biomechanical response of the eye during impact: Biomedical Science Instrumentation, v. 43, pp. 7-12.
- Kennedy, E.A., and Duma, S.M., 2008, The effects of the extraocular muscles on eye impact force-deflection and globe rupture response: Journal of Biomechanics, v. 41, pp. 3297-3302.
- Kuhn, F., Morris, F., Witherspoon, C.D., and Mester, V., 2004, The Birmingham eye trauma terminology system (BETT): J. Fr. Ophthalmology, v. 27, pp. 206-210.
- Mader, T.H., Carroll, R.D., Slade, C.S., George, R.K., Ritchey, J.P., and Neville, S.P., 2006, Ocular war injuries of the Iraq insurgency, January-September 2004. Ophthalmology, v. 113, pp. 97-104.
- Petras, J.M., Bauman, R.A., and Elsayed, N.M., 1997, Visual system degeneration induced by blast overpressure: Toxicology, v. 121, pp. 41-49.
- Pieramici, D., Sternberg, P. Aaberg, T.M et al, 1997, A system for classifying mechanical injuries of the eye (globe): American Journal of Ophthalmology, v. 123, pp. 820-831.

- Proud, W.G., Goldein, H.T., Esmail, S., and Willianson, D.M., 2009, A review of wound ballistics literature: the human body and injury processes: Security and Use of Innovative Technologies Against Terrorism (Teixeria-Das et al., Editors), Universidade de Aveiro, pp. 67-82.
- Richmond, D.R., and White, C. S., 1962, A tentative estimation of Man's tolerance to overpressures from air blast: Lovelace Foundation for Medical Education and Research, 34 p.
- Richmond, D.R., Damon, E.G., Fletcher, E.R., Bowen, I.G., and White, C.S., 1966, The relationship between selected blast-wave parameters and the response of mammals exposed to air blast: Lovelace Foundation for Medical Education and Research, 36 p.
- Richmond, D.R., Yelverton, J.T., Fletcher, E.R., and Phillips, Y.Y., 1985, Biologic response to complex blast wave: Ninth International Symposium MABS 9, Oxford, England (Los Alamos Report 20000926 077)
- Sigal, I.A., Flanagan, J.G., Tertinegg, I., and Ether, C.R., 2004, Finite element modeling of optic nerve head biomechanics: Investigative Ophthalmology and Visual Science, v. 45, pp. 4378-4387.
- Sponsel, W.E., Gray, W., Scribbick, F.W., Stern, A.R., Weiss, C.E., Groth, S.L., and Walker, J.D., 2011, Blunt eye trauma: Empirical histopathologic paintball impact thresholds in fresh mounted porcine eyes: Investigative Ophthalmology and Visual Science, v. 52, pp. 5157-5166.
- Stuhmiller, J.H., 2008a, Blast Injury: Translating research into operational medicine: Textbook of Military medicine, Borden Research Institute.
- Stuhmiller, J.H., 2008b, Blast Injury: Translating research into operational medicine: Chapter 10, Ophthalmic Care of the Combat Casualty, Textbook of Military medicine, Borden Research Institute.
- Stewart, C., 2006, Blast injuries: Preparing for the inevitable: Emergency Medicine Practice, v 8, pp. 1-28.
- Thach, et al., 1999, Ocular injuries from paintball pellets: Ophthalmology, v. 106, pp. 533-537.
- Thach, et al., 2008, Severe eye injuries in the War in Iraq, 2003-2005, Ophthalmology, v. 115, pp. 377-382.
- Uchio, E., Ohno, S. Kudoh, J., Aoki, K., Andoh, K., and Kisielewicz, L.T., 1999, Simulation model of an eye based on finite element analysis on a supercomputer: British Journal of Ophthalmology, v. 83, pp. 1106-111.

Weichel, E.D., Colyer, M.H., Baustista C., Bower, K.S., and French, L.M., 2009,
Traumatic brain injury associated with combat ocular trauma: Journal of Head
Trauma Rehabilitation, v. 24, pp. 41-50.

APPENDIX I

Porcine Eye Blast Experiments Matrix

Randomized Porcine Eye Test Matrix

Anticipated Date	Driver Volume	Burst Disks	Target Press(psi)	Anticipated Date	Driver Volume	Burst Disks	Target Press(psi)	Anticipated Date	Driver Volume	Burst Disks	Target Press(psi)
1/10/2013	1	1	7	2/28/2013	1	2	12	4/18/2013	2	4	17
1/10/2013	1	4	17	2/28/2013	1	2	12	4/18/2013	2	7	25
1/10/2013	1	2	12	2/28/2013	1	5	19	4/18/2013	2	1	7
1/10/2013	1	7	25	2/28/2013	1	6	22	4/18/2013	2	5	19
1/17/2013	1	5	19	3/7/2013	1	4	17	4/25/2013	2	7	7
1/17/2013	1	7	25	3/7/2013	1	2	12	4/25/2013	2	3	14
1/17/2013	1	6	22	3/7/2013	1	3	14	4/25/2013	2	6	22
1/17/2013	1	6	22	3/7/2013	1	3	14	4/25/2013	2	2	12
1/24/2013	1	7	25	3/14/2013	1	4	17	5/2/2013	2	5	19
1/24/2013	1	1	7	3/14/2013	1	1	7	5/2/2013	2	2	12
1/24/2013	1	5	19	3/14/2013	1	1	7	5/2/2013	2	3	14
1/24/2013	1	2	12	3/14/2013	1	7	25	5/2/2013	2	3	14
1/31/2013	1	5	19	3/21/2013	1	3	14	5/9/2013	2	4	17
1/31/2013	1	7	25	3/21/2013	1	6	22	5/9/2013	2	1	7
1/31/2013	1	6	22	3/21/2013	2	5	19	5/9/2013	2	4	17
1/31/2013	1	4	17	3/21/2013	2	2	12	5/9/2013	2	4	17
2/7/2013	1	5	19	3/28/2013	2	2	12	5/16/2013	2	2	12
2/7/2013	1	4	17	3/28/2013	2	7	25	5/16/2013	2	5	19
2/7/2013	1	3	14	3/28/2013	2	1	7	5/16/2013	2	7	25
2/7/2013	1	3	14	3/28/2013	2	4	17	5/16/2013	2	1	7
2/14/2013	1	1	7	4/4/2013	2	5	19	5/23/2013	2	4	17
2/14/2013	1	1	7	4/4/2013	2	2	12	5/23/2013	2	3	14
2/14/2013	1	7	25	4/4/2013	2	5	19	5/23/2013	2	6	22
2/14/2013	1	2	12	4/4/2013	2	6	22	5/23/2013	2	6	22
2/21/2013	1	5	19	4/11/2013	2	3	14	5/30/2013	2	7	25
2/21/2013	1	3	14	4/11/2013	2	6	14	5/30/2013	2	3	14
2/21/2013	1	4	17	4/11/2013	2	1	7	5/30/2013	2	7	25
2/21/2013	1	6	22	4/11/2013	2	6	22	5/30/2013	2	1	7

Notes: 1= normal shock tube driver volume; 2 = double shock tube driver volume (note double driver volumes result in damage to shock tube facility, thus we are currently considering other alternatives)

APPENDIX II

Summary of Porcine Blast Experiments and Observed Trauma

Disk refers to the number of aluminum or Mylar sheets used in the driver section of the shock tube. The larger the number of disks, the greater is the peak pressure, specific impulse, and energy of the blast wave.

Summary of Observed Trauma – 6 Disk at 42 cm

Experiment Set	20130411-1	20130411-2	20130411-2	20130417-6	20130502-1	20130502-4	20130502-5	20130711-3'
Eye #	1	2	1	6	1	4	5	3
Purpose	Shot	Shot	Shot	Shot	Shot	Shot	Shot	Shot
Orientation	Right	Right	Right	Right	Right	Right	Right	Left
Pre-Inflation (g)	11.7	11.4	6.4	6.3	8.7	8.2	6.6	
Post-Inflation (g)	12.3	11.5	6.5	6.3	8.7	8.4	6.8	7.3
Inflation Method	Pars Plana	Pars Plana	Pars Plana	Pars Plana	Pars Plana	Pars Plana	Pars Plana	Pars Plana
Raised IOP (mmHg)	87	86	22	46	82	37	85	87
Pre- Blast IOP (mmHg)	10	9	13	32	22	10	51	18
Post Blast-IOP (mmHg)	9	6	5	*too low to	14	6	27	9
Post-Blast Storage	Hank's BSS	Hank's BSS	Hank's BSS	Hank's BSS	Hank's BSS	Hank's BSS	Hank's BSS	Hank's BSS
Exposed Area (sq meter)	0.00049564	0.00045262	0.00042862	0.0003976	0.00046807	0.00044155	0.0003648	0.000292
# Discs	6	6	6	6	6	6	6	6
Reference P_Max (kPa)	199.9	207.4	242.5	245.9	238.6	256.5	214.3	238.4
Reference Duration (ms)	3.54	3.45	3.43	3.56	3.46	3.49	3.52	4.36
Reference Impulse (Pa-sec)	270.1	267.9	285.9	272.8	299	309.3	291.5	323.6
Total P_Max (kPa)	432.6	472.3	554.1	602.3	587	617.9	487.2	518.1
Total Impulse (Pa-s)	487.2	502.1	558.9	522.8	593.9	638.7	564.7	587
Total Duration (ms)	4.14	4.01	4.26	4.08	4.44	4.24	4.48	4.3
Energy (J)	2.370348205	2.24553634	4.41438016	3.42920434	4.44118655	4.73417523	3.1207138	2.01228296
Angle	1	0	0	1	0	0	0	0
Anterior Chamber	0	0	0	0	0	0	0	0
Choroid	0	2	2	0	0	0	0	4
Chorioretina	2	2	2	2	0	0	0	4
Cornea	0	0	0	0	0	0	0	0
Iris	0	0	0	0	0	0	0	0
Lamina Cribosa	0	0	0	0	0	0	0	0
Lens	0	0	0	0	0	0	0	0
Optic Nerve	0	1	2	0	0	0	0	3
Retina	1	2	1	1	0	0	0	4
Sclera	0	0	0	0	0	0	0	1

Summary of Observed Trauma – 6 Disk

Experiment Set	20130110-4	20130124-5	20130131-7	20130613-1	20130620-1
Eye #	4	5 (e?)	7	1	1
Purpose	Shot	Shot	Shot	Shot	Shot
Orientation	Right	Right	Right	Left	Right
Pre-Inflation (g)				10.4	9
Post-Inflation (g)	6.39975	8.03525	5.0745	10.5	9
Inflation Method	Anterior Cha	Anterior Cha	Anterior Cha	Pars Plana	Pars Plana
Raised IOP (mmHg)	23	13	65	51	74
Pre- Blast IOP (mmHg)	4	4	12	5	14
Post Blast-IOP (mmHg)		*too low to	5	*too low to	9
Post-Blast Storage	Plastic Bag	Plastic Bag	Plastic Bag	Hank's BSS	Hank's BSS
Exposed Area (sq meter)	0.00025599	0.00032141	0.00020298	0.00052621	0.00052087
# Discs	6	6	6	6	6
Reference P_Max (kPa)	151.8	155.8	147.2	147.5	155.3
Reference Duration (ms)	2.76	2.78	2.72	2.79	2.9
Reference Impulse (Pa-sec)	190.6	193.5	188.9	186.9	190
Total P_Max (kPa)	289	287.5	289.2	290	307.8
Total Impulse (Pa-s)	289	294.8	286.3	286	291.7
Total Duration (ms)	3.11	3.16	3.14	3.33	3.35
Energy (J)	0.42761082	0.55865583	0.33275603	1.07852686	1.28250493
Angle	0	2	0	0	0
Anterior Chamber	0	0	0	0	0
Choroid	4	0	2	3	0
Chorioretina	4	0	2	3	0
Cornea	0	0	0	0	0
Iris	0	0	0	0	0
Lamina Cribosa	0	0	0	0	0
Lens	0	0	0	0	0
Optic Nerve	4	0	0	0	0
Retina	4	0	2	3	0
Sclera	1	1	3	3	0

Summary of Observed Trauma – 5 Disk

Experiment Set	20130110-3	20130117-2	20130124-7	20130207-8	20130405-1	20130606-1	20130613-2
Eye #	3	2	7	8	1	1	2
Purpose	Shot	Shot	Shot	Shot	Shot	Shot	Shot
Orientation	Right		Right		Left	Right	Right
Pre-Inflation (g)					8.1	8.6	9.9
Post-Inflation (g)	6.944	5.064	7.24175	8	8.5	8.7	9.9
Inflation Method	Anterior Chamber	Anterior Chamber	Anterior Chamber	Pars Plana	Pars Plana	Pars Plana	Pars Plana
Raised IOP (mmHg)	17	9	43	24	87	58	85
Pre- Blast IOP (mmHg)	5	4	7	42	13	5	44
Post Blast-IOP (mmHg)			6		9	6	31
Post-Blast Storage	Plastic Bag	Plastic Bag	Plastic Bag	Hank's BSS	Hank's BSS	Hank's BSS	Hank's BSS
Exposed Area (sq meter)	0.00027776	0.00020256	0.00028967	0.00032	0.00030454	0.00049362	0.0004078
# Discs	5	5	5	5	5	5	5
Reference P_Max (kPa)	152.4	134.3	138.9	137.8	126.1	140	135.2
Reference Duration (ms)	2.67	2.58	2.68	2.5	2.5	2.79	2.61
Reference Impulse (Pa-sec)	162.8	165.5	171.4	158.1	147.8	169.5	164.7
Total P_Max (kPa)	251.1	256.8	259.6	271.3	221.6	271.4	248.9
Total Impulse (Pa-s)	238.4	239.8	252.7	230.7	210.9	253.8	242.3
Total Duration (ms)	3.01	3.07	3.1	3.11	2.96	3.15	3.05
Energy (J)	0.31572735	0.23296037	0.36995082	0.34062394	0.24265706	0.90202689	0.4929803
Angle	0	0	2	0	3	0	0
Anterior Chamber	0	0	0	0	3	0	0
Choroid	4	4	0	0	4	0	0
Chorioretina	4	4	2	1	4	0	1
Cornea	0	0	0	0	0	0	0
Iris	0	0	0	0	2	0	0
Lamina Cribosa	0	0	0	0	0	0	0
Lens	0	0	0	0	1	0	0
Optic Nerve	2	4	4	0	3	0	0
Retina	3	4	4	1	3	0	0
Sclera	3	2	2	1	0	0	1

Summary of Observed Trauma – 4 Disk

Experiment Set	20130117-4	20130131-3	20130405-2	20130606-3	20130613-4	20130620-2
Eye #	4	3	2	3	4	2
Purpose	Shot	Shot	Shot	Shot	Shot	Shot
Orientation	Right	Left	Right	Left	Left	Left
Pre-Inflation (g)			7.7	8.5	8.2	10.2
Post-Inflation (g)	5.8735	5.65025	8.3	8.8	8.3	10.5
Inflation Method	Anterior Cha	Anterior Cha	Pars Plana	Pars Plana	Pars Plana	Pars Plana
Raised IOP (mmHg)	11	48	64	84	84	54
Pre- Blast IOP (mmHg)	24	9	6	11	14	5
Post Blast-IOP (mmHg)		*too low to	4	9	11	5
Post-Blast Storage	Plastic Bag	Plastic Bag	Hank's BSS	Hank's BSS	Hank's BSS	Hank's BSS
Exposed Area (sq meter)	0.00023494	0.00022601	0.00034767	0.00054458	0.00049454	0.00053059
# Discs	4	4	4	4	4	4
Reference P_Max (kPa)	119.2	136.6	113.1	117.3	116.1	122.9
Reference Duration (ms)	2.56	2.49	2.42	2.55	2.58	2.53
Reference Impulse (Pa-sec)	136.4	146.8	128.4	143.8	143.3	144.1
Total P_Max (kPa)	214.9	233.1	191	209.2	215	221.2
Total Impulse (Pa-s)	190.5	207.4	177.2	203.6	203.2	206.8
Total Duration (ms)	2.99	2.97	2.93	2.99	2.97	3.02
Energy (J)	0.17052063	0.19443532	0.22864083	0.69849975	0.60833411	0.5733237
Angle	0	4	4	0	0	0
Anterior Chamber	1	2	4	0	0	0
Choroid	2	2	4	0	0	3
Chorioretina	2	2	4	0	0	3
Cornea	0	0	0	0	0	0
Iris	0	0	0	0	0	0
Lamina Cribosa	0	0	0	0	0	0
Lens	0	0	1	0	0	0
Optic Nerve	0	0	4	0	0	3
Retina	1	4	4	0	0	0
Sclera	1	4	2	0	0	3

Summary of Observed Trauma – 3 Disk

Experiment Set	20130110-2	20130131-2	20130405-5	20130606-4	20130613-5	20130620-5
Eye #	2	2	5*	4	5	5
Purpose	Shot	Shot	Shot	Shot	Shot	Shot
Orientation	Right	Right	Right	Right	Right	Right
Pre-Inflation (g)			6.9	8.4	8.3	7.7
Post-Inflation (g)	5.28425	5.04	7.6	8.4	8.1	7.7
Inflation Method	Anterior Cha	Anterior Cha	Pars Plana	Pars Plana	Pars Plana	Pars Plana
Raised IOP (mmHg)	17	37	23	56	85	74
Pre- Blast IOP (mmHg)	14	9	5	10	8	9
Post Blast-IOP (mmHg)		5	4	9	6	10
Post-Blast Storage	Plastic Bag	Plastic Bag	Hank's BSS	Hank's BSS	Hank's BSS	Hank's BSS
Exposed Area (sq meter)	0.00021137	0.0002016	0.00034917	0.00043689	0.00049647	0.00047815
# Discs	3	3	3	3	3	3
Reference P_Max (kPa)	99.6	99.8	90	101.2	98.5	101.8
Reference Duration (ms)	2.44	2.43	2.39	2.47	2.48	2.47
Reference Impulse (Pa-sec)	113	114.5	100.4	116.1	116.8	119
Total P_Max (kPa)	170.3	184.5	158.7	176	172.6	174.6
Total Impulse (Pa-s)	147.7	150.1	130.7	157.2	157.1	160.9
Total Duration (ms)	2.64	2.89	2.65	2.75	2.72	2.74
Energy (J)	0.09222196	0.090841	0.1370192	0.28076309	0.37551162	0.38434363
Angle	0	0	0	0	0	0
Anterior Chamber	0	0	0	0	0	0
Choroid	1	0	0	3	4	0
Chorioretina	1	0	0	3	4	0
Cornea	0	0	0	0	0	0
Iris	0	0	0	0	0	0
Lamina Cribosa	0	0	0	0	0	0
Lens	0	0	0	0	0	0
Optic Nerve	1	0	0	2	4	0
Retina	1	0	0	3	4	0
Sclera	0	0	0	0	4	0

Summary of Observed Trauma – 2 Disk

Experiment Set	20130124-2	20130131-4	20130307-6	20130405-6	20130502-7	20130606-5	20130620-6
Eye #	2	4	6	6'	2	5	6
Purpose	Shot	Shot	Shot	Shot	Shot	Shot	Shot
Orientation	Right	Right	Left	Left	Right	Right	Left
Pre-Inflation (g)			8.9	7.1	7.9	8.7	9.3
Post-Inflation (g)	8.04275	5.15375	8.90775	7.3	7.9	8.7	9.5
Inflation Method	Anterior Chamber	Anterior Chamber	Pars Plana				
Raised IOP (mmHg)	*too high to	34	56	89	86	85	47
Pre- Blast IOP (mmHg)	8	5	18	10	15	10	5
Post Blast-IOP (mmHg)	7	*too low to	13	6	10	4	9
Post-Blast Storage	Plastic Bag	Plastic Bag	Hank's BSS				
Exposed Area (sq meter)	0.00032171	0.00020615	0.00035631	0.00035505	0.00040219	0.0005036	0.0004843
# Discs	2		2	2	2	2	2
Reference P_Max (kPa)	82.8		78.1	70.4	116.1	78	77.7
Reference Duration (ms)	2.35		2.26	2.32	3.08	2.39	2.3
Reference Impulse (Pa-sec)	93.61		88.46	80.61	140.3	86.71	86.54
Total P_Max (kPa)	144.7	140.3	139.1	129	242.3	142	138.3
Total Impulse (Pa-s)	116.8	112.1	111.3	99.96	204.5	111.2	110.7
Total Duration (ms)	2.55	2.46	2.48	2.42	3.33	2.65	2.64
Energy (J)	0.0877769	0.05181131	0.08827716	0.08627375	0.42814618	0.18023194	0.1512637
Angle	0	0	0	0	0	0	0
Anterior Chamber	0	0	0	0	0	0	0
Choroid	0	2	0	0	0	0	0
Chorioretina	0	2	1	0	0	0	1
Cornea	0	0	0	0	0	0	0
Iris	0	0	0	0	0	0	0
Lamina Cribosa	0	0	0	0	0	0	0
Lens	0	0	0	0	0	0	0
Optic Nerve	0	0	0	0	0	0	0
Retina	0	2	0	0	0	1	0
Sclera	0	0	0	0	0	0	1

Summary of Observed Trauma – 1 Disk

Experiment Set	20130110-1	20130117-3	20130307-5	20130328-7
Eye #	1	3	5**	7*
Purpose	Shot	Shot	Shot	Shot
Orientation	Left		Left	Right
Pre-Inflation (g)			8	8.3
Post-Inflation (g)	6.912	5.34725	11.0705	8.5
Inflation Method	Anterior Chamber	Anterior Chamber	Pars Plana	Pars Plana
Raised IOP (mmHg)	22	19	49	87
Pre- Blast IOP (mmHg)	4		38	69
Post Blast-IOP (mmHg)		6	45	44
Post-Blast Storage	Plastic Bag	Plastic Bag	Hank's BSS	Hank's BSS
Exposed Area (sq meter)	0.00027648	0.00021389	0.00044282	0.00026661
# Discs	1	1	1	1
Reference P_Max (kPa)	49.3	47.4	50.2	46.3
Reference Duration (ms)	2.15	2.23	2.08	2.07
Reference Impulse (Pa-sec)	52.98	53.37	52.2	48.31
Total P_Max (kPa)	91.9	86	96.4	79.7
Total Impulse (Pa-s)	60.27	61.04	60.21	55.65
Total Duration (ms)	2.22	2.26	2.17	2.18
Energy (J)	0.02008612	0.01593858	0.03210661	0.01294894
Angle	0	0	3	0
Anterior Chamber	0	0	2	0
Choroid	2	3	0	0
Chorioretina	2	2	0	0
Cornea	0	0	0	0
Iris	0	0	0	0
Lamina Cribosa	0	0	0	0
Lens	0	0	0	0
Optic Nerve	2	2	0	0
Retina	2	2	0	0
Sclera	0	1	0	0

Summary of Observed Trauma – Mylar Disk

Experiment Set	20130117-6	20130124-6	20130307-7	20130328-2	20130606-6
Eye #	6	6	7	2*	6
Purpose	Shot	Shot	Shot	Shot	Shot
Orientation	Right	Right	Right	Right	Right
Pre-Inflation (g)			9.5	7.5	7.7
Post-Inflation (g)	7.12175	6.525	10.97925	8	7.7
Inflation Method	Anterior Chamber	Anterior Chamber	Pars Plana	Pars Plana	Pars Plana
Raised IOP (mmHg)	57	44	47	87	-
Pre- Blast IOP (mmHg)	9	8	38	4	10
Post Blast-IOP (mmHg)	6	6	29	*too low to	-
Post-Blast Storage	Plastic Bag	Plastic Bag	Hank's BSS	Hank's BSS	Hank's BSS
Exposed Area (sq meter)	0.00028487	0.000261	0.00043917	0.00037511	0.00051186
# Discs	0.5	0.5	0.5		0.5
Reference P_Max (kPa)	23.8	21.8	42.3		37.6
Reference Duration (ms)	2.12	2.16	2.07		2.23
Reference Impulse (Pa-sec)	27.36	26.7	44.87		41.46
Total P_Max (kPa)	49.1	48.6	85.4	55.5	76.2
Total Impulse (Pa-s)	29.58	28.75	51.16	30.05	48.35
Total Duration (ms)	2.23	2.19	2.21	2.09	2.28
Energy (J)	0.00498509	0.00431466	0.02298919	0.0079412	0.03977174
Angle	0	0	2	0	0
Anterior Chamber	0	0	2	0	0
Choroid	0	4	2	0	0
Chorioretina	0	4	2	0	1
Cornea	0	0	0	0	0
Iris	0	0	0	0	0
Lamina Cribosa	0	0	0	0	0
Lens	0	0	1	0	0
Optic Nerve	0	3	3	0	0
Retina	0	4	3	0	0
Sclera	0	0	4	0	0

Summary of Observed Trauma – Controls

Experiment Set	20130110-5	20130117-5	20130124-8	20130131-1	20130307-8	20130328-64a	20130328-64b	20130405-7	20130411-4	20130417-8	20130502-8	20130613-6	20130620-8
Eye #	5	5	8	1	8	6,4a	6,4b	7	4	8	8	6	8
Purpose	Shock Tube	Shock Tube	Shock Tube	Shock Tube	Shock Tube	Shock Tube C	Shock Tube C	Shock Tube	Shock Tube	Shock Tube	Shock Tube	Shock Tube	Shock Tube
Orientation	Right	Left		Right	Left	Right	Right	Right	Right	Right	Left		Right
Pre-Inflation (g)					9.9	7.3	7.8	7.7	12.4	6.6	8.2	7.4	7.2
Post-Inflation (g)						7.6	8	8.3	12.5	6.9	8.2	7.4	7.2
Inflation Method	Anterior Cha	Anterior Cha	Anterior Ch	Anterior Ch	Pars Plana	Pars Plana	Pars Plana	Pars Plana	Pars Plana	Pars Plana	Pars Plana	Pars Plana	Pars Plana
Raised IOP (mmHg)	27	9	41	38	39	87	98	44	86	61		85	78
Pre- Blast IOP (mmHg)	*too low to	5	10	12	*too low to	14	6	6	20	6	12	12	24
Post Blast-IOP (mmHg)		4	8	11	*too low to	10	4	4	13	*too low to	10	12	12
Post-Blast Storage	Plastic Bag	Plastic Bag	Plastic Bag	Plastic Bag	Hank's BSS	Hank's BSS	Hank's BSS	Hank's BSS	Hank's BSS	Hank's BSS	Hank's BSS	Hank's BSS	Hank's BSS
Exposed Area (sq meter)	0.00023117	0.00021389	0.00032233	0.00020802	0.00059998	0.00036811	0.00036921	0.00031351	0.00043906	0.00036963	0.0003225	0.0003748	0.0005271
# Discs	0	0	0	0	0	0	0	0	0	0	0	0	0
Reference P_Max (kPa)	0	0	0	0	0	0	0	0	0	0	0	0	0
Reference Duration (ms)	0	0	0	0	0	0	0	0	0	0	0	0	0
Reference Impulse (Pa-sec)	0	0	0	0	0	0	0	0	0	0	0	0	0
Total P_Max (kPa)	0	0	0	0	0	0	0	0	0	0	0	0	0
Total Impulse (Pa-s)	0	0	0	0	0	0	0	0	0	0	0	0	0
Total Duration (ms)	0	0	0	0	0	0	0	0	0	0	0	0	0
Energy (J)	0	0	0	0	0	0	0	0	0	0	0	0	0
Angle	0	0	0	0	0	4	0	0	0	0	0	0	0
Anterior Chamber	0	0	0	0	0	0	0	0	0	0	0	0	0
Choroid	2	0	0	0	0	1	0	3	3	3	0	0	0
Chorioretina	2	0	0	0	0	1	0	3	3	3	0	0	0
Cornea	0	0	0	0	0	0	0	0	0	0	0	0	0
Iris	0	0	0	0	0	0	0	0	0	0	0	0	0
Lamina Cribosa	0	0	0	0	0	0	0	0	0	0	0	0	0
Lens	0	0	0	0	0	0	0	0	0	0	0	0	0
Optic Nerve	3	0	0	0	0	0	0	1	3	2	0	0	0
Retina	2	0	0	0	0	1	0	3	3	4	0	0	0
Sclera	1	0	0	0	1	4	0	0	0	0	0	0	0